Gene co-expression analyses of health(span) across multiple species

Steffen Möller[1*], Nadine Saul[2], Israel Barrantes[1], András Gézsi[3], Michael Walter[4], Péter Antal[3], Georg Fuellen[1]

[1] Rostock University Medical Center, Institute for Biostatistics and Informatics in Medicine and Ageing Research, Rostock, Germany
[2] Humboldt-University of Berlin, Institute of Biology, Berlin, Germany
[3] Budapest University of Technology and Economics, Department of Measurement and Information Systems, Budapest, Hungary
[4] Rostock University Medical Center, Institute for Clinical Chemistry and Laboratory Medicine, Rostock, Germany

*corresponding author

Abstract: *Health(span)-related gene clusters/modules were recently identified based on knowledge about the cross-species genetic basis of health, to interpret transcriptomic datasets describing health-related interventions. However, the cross-species comparison of health-related observations reveals a lot of heterogeneity, not least due to widely varying health(span) definitions and study designs, posing a challenge for the exploration of conserved healthspan modules and, specifically, their transfer across species.*

To improve the identification and exploration of conserved/transferable healthspan modules, here we apply an established workflow based on gene co-expression network analyses employing GEO/ArrayExpress data for human and animal models, and perform a comprehensive meta-analysis of the resulting modules related to health(span), yielding a small set of health(span) candidate genes, backed by the literature.

For each experiment, WGCNA (weighted gene correlation network analysis) was thus used to infer modules of genes which correlate in their expression with a "health phenotype score" and to determine the most-connected (hub) genes for each such module, and their interactions. After mapping these hub genes to their human orthologs, 12 health(span) genes were identified in at least two species (ACTN3, ANK1, MRPL18, MYL1, PAXIP1, PPP1CA, SCN3B, SDCBP, SKIV2L, TUBG1, TYROBP, WIPF1), for which enrichment analysis by g:profiler finds an association with actin filament-based movement and associated organelles as well as muscular structures.

We conclude that a meta-study of hub genes from co-expression network analyses for the complex phenotype health(span), across multiple species, can yield molecular-mechanistic insights and can direct experimentalists to further investigate the contribution of individual genes and their interactions to health(span).

Introduction

Health and healthspan are gaining acceptance as central concepts in medicine, with a focus on (multi-)morbidity, aiming to delay the onset of disease and dysfunction for as long as possible. Health is difficult to describe and has different meanings to different people. Aging, and the deterioration of health that comes with it, affects nearly all species. But tissues that enable the systematic study of the underlying molecular processes are more easily available for animal models, especially for invertebrates, coming with further advantages such as

controlled genetics and environments, and a much shorter lifespan. Thus, aging and healthspan are frequently studied in animal models.

To support aging research, many databases are now available (Tacutu *et al.*, 2018). Gene expression profiles across tissues of aging mice were already presented, e.g., by the AGEMAP (Zahn *et al.*, 2007) project in 2007 and recently by the Aging Atlas Consortium (2020), but there is a lack of such data for healthspan. Adding the dimension of health may amend the identification of molecular markers for aging and further support the identification of health-modulatory compounds (Dönertaş *et al.*, 2018).

An increasing number of transcriptomic data sets that can be used to compare young and old individuals are available on public repositories. The concept to derive aging-associated patterns from transcriptome repositories across species (de Magalhães *et al.*, 2009) already led to central elements of aging-related knowledge bases (Tacutu *et al.*, 2012 and 2018). Comprehensive analyses of transcriptome repositories were also expanded towards diseases in the context of aging (van Dam *et al.*, 2012). Yet, as for expression profiles *per se*, there is a lack of gene expression co-regulation analyses across species with a focus on health(span). A major challenge for polygenic phenotypes in general is the heterogeneity of the underlying gene regulatory landscape (Kotlyar *et al.*, 2019), impeding the use of network-based methods for post-processing, i.e., smoothing, aggregating, and unifying, transcriptomic results (Leiserson *et al.*, 2013; Cowen *et al.*, 2017). However, the power of the cross-species derivation of conserved co-regulation modules is becoming apparent, see, e.g., the CoCoCoNet database (Lee *et al.*, 2020).

For prominent cellular characteristics of aging, such as cellular senescence, Avelar and coworkers (2020) demonstrated how to integrate static data from public databases with insights from gene co-expression (https://coxpresdb.jp/, Obayashi *et al.*, 2019). Attempts were also made to use known gene/protein interactions to describe age-induced expression profiles (Faisal and Milenković, 2014). The integration of co-expression data, also across species, could similarly be performed with GeneFriends (van Dam *et al.*, 2015, for human and mouse) for RNA-seq or, for microarray data also with MIM (Adler *et al.*, 2009). The latter also provides provenance information, i.e. the experimental context in which the correlation was found, to plan follow-up experiments.

We recently proposed an operational definition of health (Fuellen *et al.*, 2019) and suggested that it may be applied across species. We then collected data on molecular contributions to health (Möller *et al.*, 2020), with a focus on genetics. With the support of GeneMania (Franz *et al.*, 2018) and the associated tool AutoAnnotate (Kucera *et al.*, 2016) we then constructed a map of network modules by clustering a functional interaction network of the genes implicated in health. Naturally, aging and health are complex phenotypes for which we still lack the means to single-out and investigate the contribution of individual genes. Any detailed analysis is therefore expected to dissect a list of health-associated genes into gene sets that, in turn, can be understood as parts of the whole (that is health), and these parts are distributed across diseases & dysfunctions, tissues & organs, and species. The idea of identifying health-associated molecular patterns is at the root of molecular health research. Our efforts strived for a consensus across the species barrier of worm (*Caenorhabditis elegans*) and humans and we investigated the transfer of findings from worm as a short-lived

animal model of health to humans. A consensus in network modules of worm and human was thus determined (Möller *et al.*, 2020), but it was small in relation to the much larger functional interaction networks that were the starting point for each species. However, functional interaction databases, upon which GeneMania is based, are woefully incomplete. Also, these databases do not usually consider the specific biological context of an interaction, but instead merge interaction data from very heterogeneous sets of experiments (Magger *et al.*, 2012; Kotlyar *et al.*, 2019).

To harness the power of diverse transcriptomic experiments in the context of health(span), here we present a WGCNA-based meta-study for the exploration and characterization of health(span) related modules. WGCNA co-expression analyses have recently been used in aging research (Li *et al.*, 2019) to identify differences in old vs young and gene expression asymmetries *in the brain* that develop over time. In our study we integrated a very diverse set of health(span) expression data across species from many different tissues. We manually derived a scoring for all the transcriptome samples we consider, based on a score combining quantitative and qualitative factors that the authors of the experiments provided and refer to it as their “health phenotype score”. WGCNA was found to be a competitive tool to find network modules reflecting such kinds of scores (van Dam *et al.*, 2017). Across tissues (or cell lines) and multiple species, this allows the filtering for health-associated modules generated by the WGCNA correlation analysis and thus, the meta-study of health-associated most-connected genes (hubs) and of their interactions, as presented here. We also collected the evidence for the implication of these genes in health(span) from the literature.

Methods

All sets of transcriptomics experiments in the Gene Expression Omnibus (GEO, Clough and Barrett, 2016) and ArrayExpress (Athar *et al.*, 2019) databases that mention “healthspan” in the title or the description were included, if they featured more than 6 samples and a scale-free network could be derived from their correlation matrix (for the latter, see below). Experiments performed on *C. elegans* were added when these were alternatively annotated with the term “health”, to increase the number of datasets for the worm, since ‘healthspan and "Caenorhabditis elegans"’ only finds the single entry E-GEOD-54853. We did not include *non*-worm experiments with “health” in the title or the description, since the number of matches (specifically for human) turned out to be excessively large.

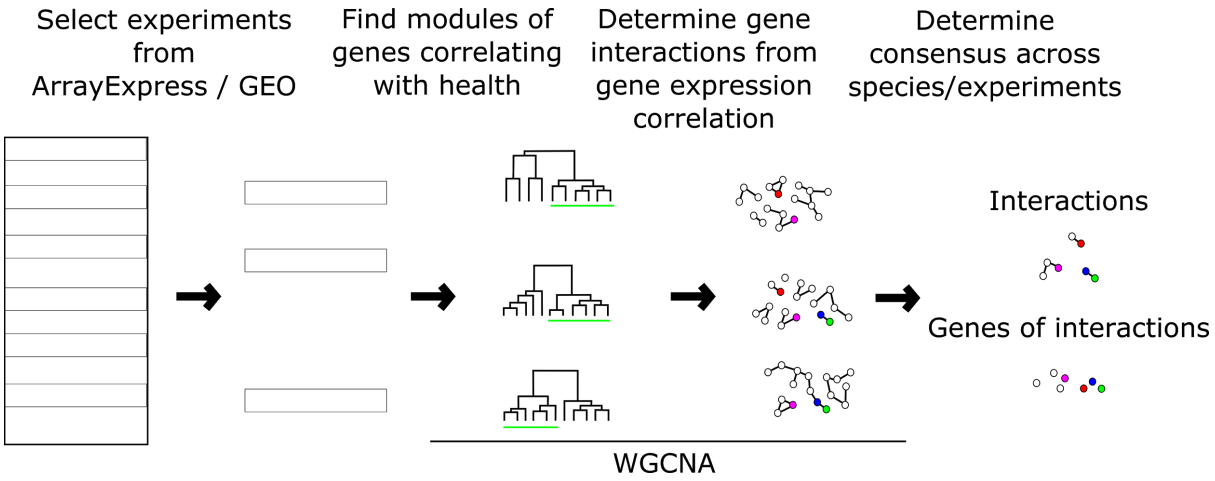

Figure 1: Workflow to determine cross-species consensus gene correlation networks, and subsequent analyses. *WGCNA is applied independently for each selected experiment in ArrayExpress/GEO, defining modules and gene interactions. Gene interactions are filtered by experiment-specific thresholds. For each module, hub genes are retrieved and those with an ortholog found as a hub gene in another species are reported in Table 2. For each module, Table 3 lists the genes that correlate the most with its "eigengene", i.e. that best represent the module's expression pattern across samples.*

Each experiment's metadata was inspected to manually derive a score designed to reflect the health status of the individual(s) from which the sample(s) were taken, unless such a score was already given. This "health phenotype score" was manually tailored for each experiment by a custom formula that takes the experiment's factor annotation as an input and thus consistently annotates each sample. This can be inspected in the 'Data_parameters' folder (see Availability). Log-transformation of expression levels was performed if not already performed for the data we retrieved. Table 1 describes the experimental data and metadata which form the input to the following analyses.

Table 1: List of ArrayExpress/GEO files used as input in our study. *This table provides an overview of the transcriptomics experiments that were retrieved for this study. Each experiment was processed by a regular WGCNA workflow with unsigned correlation. Interactions were collected for the 30 most connected (hub) genes in each module. The column Modules lists the number of modules found for the experiment that feature an eigengene that correlates (with P<0.05) with the samples' health phenotype score. Within each module, only interactions with an adjacency value above the 95th percentile of an experiment were considered. The rightmost column lists the number of different hub genes that are paired in any of these interactions. Numbers in parentheses give the number of genes/interactions that could be mapped to ortholog genes in the human; for human data, the number of orthologs in worm are shown. For an interaction, both of the paired genes need to have orthologs assigned; otherwise they were not considered for the count.*

Group	Accession (Technology)	Analysed treatment-groups	Description	number of (with orthologs)			
				Samples[1] [total / per group]	Modules	Interactions	Genes
HEALTHS	E-GEOD-19102 (array)	i) high-fat diet + 100mg/kg SRT1720, ii) high-fat diet + 30mg/kg SRT1720, iii) high-fat diet, iv) standard AIN-93G diet	An activator of Sirt1, SRT1720, extends healthspan and lifespan in diet-induced obese mice; samples: liver tissue from strain C57BL/6J	12/3	10	324 (182)	28 (20)

PANMOUSE	E-GEOD-34773 (array)	i) PGC-1a skeletal muscle specific knockout, ii) PGC-1a skeletal muscle specific knockout + CR, iii) WT, iv) WT + CR	PGC-1a is a transcriptional coactivator that regulates mitochondrial function and is induced by CR; PGC-1a mediates mitochondrial, but not metabolic, changes during calorie restriction (Finley *et al.*, 2012)	26/6-7	12	0 (0)	0 (0)
	E-GEOD-40936 (array)	i) ad libitum diet, muscle tissue, ii) ad libitum diet + 0.1% w/w metformin, muscle tissue, iii) 40% calorically restricted diet, muscle tissue, iv) ad libitum diet, liver tissue, v) ad libitum diet + 0.1% w/w metformin, liver tissue, vi) 40% calorically restricted diet, liver tissue	Chronic treatment with low dose of metformin (0.1% w/w in diet) starting at one year of age extends health and lifespan in male mice, while a higher dose (1% w/w) was toxic	30/5	1	434 (0)	29 (23)
	E-GEOD-49000 (array)	i) standard diet, muscle tissue, ii) standard diet liver tissue, iii) standard diet + SRT2104, muscle tissue, iv) standard diet + SRT2104, liver tissue, v) 40% Caloric restriction, muscle tissue, vi) 40% Caloric restriction, liver tissue	SRT2104, a synthetic small molecule activator of SIRT1, extends survival of male mice on a standard diet and preserves bone and muscle mass (Mercken *et al.*, 2014)	30/5		no modules found	
	E-GEOD-54853 (RNA-seq)	i) 10 g/kg D-Glucoseamine, ii) untreated	D-Glucoseamine mimics a ketogenic diet and extends lifespan of aging C57BL/6 mice	12/6	1	435 (0)	30 (19)
	E-GEOD-55272 (array)	i) WT, 5 months, liver tissue, ii) WT, 24 months, liver tissue, iii) WT, 5 months, muscle tissue, iv) WT, 24 months, muscle tissue, v) WT, 5 months, adipose tissue, vi) WT, 24 months, adipose tissue, vii) Myc+/- , 5 months, liver tissue, viii) Myc+/- , 24 months, liver tissue, ix) Myc+/- , 5 months, muscle tissue, x) Myc+/- 24 months, muscle tissue, xi) Myc+/- , 5 months, adipose tissue, xii) Myc+/- , 24 months, adipose tissue	The pleiotropic transcription factor MYC is a proto-oncogene and Myc+/- heterozygous mice have extended lifespan and improved healthspan	36/3	6	567 (377)	79 (64)
	E-MTAB-6578 (RNA-seq)	female heart tissue: i) 10 weeks, HGPS-/- mutants, ii) 10 weeks, HGPS-/-; NAT10-/- double mutants, iii) 10 weeks, NAT10-/- mutants, iv) 10 weeks, HGPS-/- mutants + 100 mg/kg remodelin, v) 104	Targeting NAT10 enhances healthspan and lifespan in a mouse model of human accelerated aging syndrome (Hutchinson-Gilford progeria syndrome)	12/2	1	0 (0)	0 (0)

		weeks, WT, vi) 10 weeks, WT					
RAT	E-GEOD-38062 (array)	i) fed ad libitum, ii) fed 40% CR	Muscle specimens of rats following a calorie restriction (40%) diet vs ad libitum fed rats; age: from 2-27 months (Mercken *et al.*, 2013)	10/5	8	467 (81)	57 (24)
HUMAN	E-GEOD-38012 (array)	i) middle-aged humans under CR diet, ii) middle-aged humans under western diet	Skeletal muscle specimens of humans following a calorie restriction diet vs humans following a Western diet	25/10-15	2	405 (324)	28 (25)
	E-GEOD-66236 (array)	i) adipocytes proliferating in culture, ii) adipocytes in gamma-irradiation induced senescence	Difference between senescent and non-senescent cells in order to develop senolytic drugs	16/8	1	435 (276)	30 (24)
HEALTH WORM	E-GEOD-8696 (array)	i) 4 µM, ii) 20 µM, & iii) 500 µM hemin	To understand heme homeostasis, genes transcriptionally regulated by heme should be identified (Rajagopal *et al.*, 2008)	9/3	4	22 (0)	20 (7)
	E-GEOD-9246 (array)	i) *slr-2*(ku297) mutants, ii) WT	Transcription profiling of *C. elegans slr-2* (C2H2 Zn-finger protein) mutants at L1 stage	6/3	1	434 (104)	29 (14)
	E-GEOD-9301 (array)	i) 99% O2 (oxidative stress), ii) 99% O2 + *skn-1* RNAi, iii) untreated	*C. elegans* treated with oxidative stress in absence and presence of the transcription factor SKN-1, which is involved in response to oxidative stress	11/3-4		no modules found	
	E-GEOD-21531 (array)	i) *unc-32; glp-1* double mutants (excess proliferation), ii) *unc-32* mutants	Analysis of germ cell proliferation in *unc-32*(e189);*glp-1*(oz112gf) double mutants (excess germ cell proliferation) compared to *unc-32*(e189) mutants as control (Waters *et al.*, 2010)	8/4		no modules found	
	E-GEOD-30505 (array)	i) L3, WT, EV, ii) L3, WT, *ash-2* RNAi, iii) L3, *glp-1*(e2141ts) mutants, EV, iv) L3, *glp-1*(e2141ts) mutants, *ash-2* RNAi, v) day 8, WT, EV, vi) day 8, WT, *ash-2* RNAi, vii) day 8, *glp-1*(e2141ts) mutants, EV, viii) day 8, *glp-1*(e2141ts) mutants, *ash-2* RNAi	The ASH-2 trithorax complex trimethylates histone H3 at lysine 4 (H3K4); *ash-2* knock-down increases lifespan in a germline dependent manner. *ash-2* knock-down was compared in young and old as well as in WT and germline deficient (*glp-1*) mutants (Greer et al., 2010)	23/2-3	4	854 (146)	60 (20)
	E-GEOD-32031 (array)	i) *nhr-23* RNAi, ii) untreated	Inhibition of *nhr-32*, important for growth and molting, in L2 larvae	6/3	1	124 (2)	27 (5)
	E-GEOD-32339 (array)	i) L3 WT, ii) L3 *nep-1* mutants, iii) adult WT, iv) adult *nep-1* mutants	Comparison between wild-type and *nep-1* (homologue of human ECE1 (endothelin-converting enzyme 1) mutant strain	10/2-3	3	867 (173)	57 (25)

E-GEOD-35939 (array)	embryonic touch-receptor cells with i) mutant Huntingtin (128Q) vs normal Huntingtin (19Q), ii) normal Huntingtin (19Q) vs GFP only	Comparison of purified touch receptor neurons expressing mutant Huntingtin N-terminal fragment (expanded polyGlutamine) with normal Huntingtin N-terminal fragment	12/6		no modules found	
E-GEOD-36494 (RNA-seq)	i) WT, ii) WT + TAP (tobacco acid pyrophosphatase), iii) *rde-10* mutant, iv) *rde-10* mutant + TAP, v) *rde-11* mutant, vi) *rde-11* mutant + TAP)	The RDE-10/RDE-11 complex triggers RNAi induced mRNA degradation by association with target mRNA in *C. elegans* (Yang et al., 2012)	12/2		no modules found	
E-GEOD-38877 (array)	centrifuged at i) 1g, ii) 5g, iii) 10g, iv) 15g	Worms spun in centrifuge at elevated g values	18/3-9		no modules found	
E-GEOD-40459 (array)	i) *rsd-2* (yp10) mutants, 25 °C, late generation, ii) *rsd-2* (yp10) mutants, 25 °C, early generation, iii) *rsd-2* (pk3307) mutants, 25°C, late generation, iv) *rsd-2* (pk3307) mutants, 25°C, early generation, v) *rsd-6* (pk3300) mutants, 25°C, late generation, vi) *rsd-6* (pk3300) mutants, 25°C, early generation,vii) *rsd-2* (yp10) mutants, 20 °C, late generation, viii) *rsd-2* (yp10) mutants, 20 °C, early generation, ix) *rsd-2* (pk3307) mutants, 20°C, late generation, x) *rsd-2* (pk3307) mutants, 20°C, early generation, xi) *rsd-6* (pk3300) mutants, 20°C, late generation, xii) *rsd-6* (pk3300) mutants, 20°C, early generation	Effects of transgeneration aging studied in early and late generation *rsd-2* and *rsd-6* mutants at the restrictive temperature of 25°C and the permissive temperature of 20°C	36/3		no modules found	
E-GEOD-42192 (array)	i) fed with E.coli OP50 for 3 days or ii) 10 days, iii) fed with Lactobacillus rhamnosus CNCM I-3690 for 3 days or iv) 10 days, v) fed with Lactobacillus rhamnosus CNCM I-4317 for 3 days or vi) 10 days	The lactic acid bacteria *Lactobacillus rhamnosus* (CNCM I-3690) increase worm's lifespan by antioxidative actions	18/3	2	868 (71)	58 (15)
E-GEOD-43864 (array)	i) *nhr-114* RNAi, ii) *glp-1*(q224ts) mutants, iii) WT untreated, iv) WT + tryptophan	The nuclear receptor *nhr-114*/HNF4 protects germline stem cells from dietary metabolites. The downregulation of *nhr-114* results in germline defects and sterility, which depends on tryptophan. Sterile *glp-1* mutants are used for comparison. animals	12/3	9	1287 (263)	73 (31)
E-GEOD-46051 (RNA-se	i) day 1, ii) day 1 + 100 nM rotenone, iii) day 5, iv) day 5 + 100 nM rotenone, v) day 10, vi)	Deep sequencing of endogenous mRNA from Caenorhabditis elegans in the presence and absence of	22/2-3	21	3123 (474)	264 (74)

q)	day 10 + 100 nM rotenone, vii) day 20, viii) day 20 + 100 nM rotenone	rotenone at 4 different time points (Schmeisser *et al.*, 2013)				
E-GEOD-51502 (array)	i) genetically activated beta-catenin, ii) WT	Use of an activated beta-catenin to identify Wnt/beta-catenin pathway target genes (Jackson *et al.*, 2014)	6/3	3	1302 (112)	86 (27)
E-GEOD-52340 (array)	i) WT, ii) *rsks-1* mutants, iii) *daf-2* mutants, iv) daf-2;rsks-1 double mutants, v) daf-16;daf-2;rsks-1 triple mutants	Synergistic lifespan extension in daf-2;rsks-1 double mutants requires DAF-16 and the germline was identified as the key tissue for this synergistic longevity (Chen *et al.*, 2013)	47/9-10		no modules found	
E-GEOD-54853 (RNA-seq)	i) 100 µM D-Glucosamine, ii) untreated	D-Glucosamine extends C. elegans lifespan by impairing glucose metabolism to activate AMP-activated protein kinase	12/6	2	870 (0)	60 (20)
E-GEOD-57739 (RNA-seq)	i) WT + standard food (OP50), ii) WT + *S. aureus*, iii) *hlh-30* mutants + OP50, iv) *hlh-30* mutants + *S. aureus*	HLH-30/TFEB is a transcription factor in the host response to infections and regulates the transcription of cytoprotective and antimicrobial genes (Visvikis *et al.*, 2014)	8/2		685 (55)	90 (28)
E-GEOD-85342 (array)	i) 5-fluorouracil, ii) DMSO	Treatment with 5-fluorouracil inhibits growth of *P. aeruginosa* and reduces pyoverdine biosynthesis	6/3		no modules found	
E-MEXP-479 (array)	i) fed with standard food for 12h or ii) 24h, iii) fed with *Drechmeria coniospora* for 12h or iv) 24h	Exposure to the fungal pathogen Drechmeria coniospora for 12 and 24 hours (Pujol *et al.*, 2008)	64/16		no modules found	
E-MTAB-1333 (array)	pash-1(mj100) mutants at restrictive temperature (25 °C) for i) 0, ii) 6, iii) 12 or iv) 24 hours, pash-1(mj100); pash-1::gfp mutants at 25 °C for v) 0, vi) 6, vii) 12 or viii) 24 hours	Reversible inactivation of miRNA synthesis via DGCR8/pash-1 conditional mutants (Lehrbach et al., 2012)	24/3	6	1715 (440)	119 (58)
E-MEXP-1808 (array)	i) strain DR1350, ii) strain DR1350 + dauer pheromone, iii) WT N2, iv) WT N2 + dauer pheromone	Wild type isolates treated with dauer larva-inducing pheromone (Harvey et al., 2009)	12/3		no modules found	
E-MEXP-1810 (array)	i) strain RIL-14, ii) strain RIL-14 + dauer pheromone, iii) strain RIL-17, iv) strain RIL-17 + dauer pheromone	Wild type isolates treated with dauer larva-inducing pheromone	12/3	6	261 (108)	65 (37)

[1] total: total samples in this experiment; per group: samples per treatment-group (biological replicates)

RNA-seq data re-analysis

Gene expression levels were typically not available for the RNA-seq data. Therefore, the RNA-seq datasets were all reanalyzed based on the raw data by the following protocol. All target RNA-seq datasets were retrieved from the European Nucleotide Archive (Leinonen *et al.*, 2011), and the corresponding FASTQ files were filtered for Illumina adapters, phage PhiX sequences and quality (Phred score over 25) using BBTools version 38.49 (Bushnell *et al.*, 2017). Gene expression was then quantified for each RNA-seq run. To this end, the filtered outputs were mapped against the corresponding target genomes from the Ensembl database release 98 (Yates *et al.*, 2019), using the STAR program version 2.7.3a (Dobin *et al.*, 2013). This program also enabled us to assign uniquely mapped reads to individual genes from the short read alignments. Finally, the mapped read counts were normalized as transcripts per million (Li *et al.*, 2010).

Network analysis

For each experiment, gene interactions are derived from their pairwise Pearson-correlation of gene expression across samples with the WGCNA (Langfelder and Horvath, 2008; Zhao *et al.*, 2010) R package. The WGCNA analysis was performed for undirected interactions. Parameters were set as instructed by the WGCNA standard protocol, as follows. For every experiment the *cutHeight* was manually set to remove outliers and the exponent/power was manually determined to ensure that the network is a scale-free network (see below). An experiment is skipped if that is not possible and then marked with “no modules found” in Table 1. For RNA-seq, prior to the removal of outliers, low-count genes were removed by a manual setting of the parameter *cutHeight* so that the separation of the samples reflects their phenotypes and could no longer be improved, based on the clustering of the genes by expression data with the R function *hclust* as performed as part of the WGCNA protocol.

In an attempt to make the correlation networks of different experiments more similar to each other with respect to the number of connections that may be expected for each gene, we adhered to the WGCNA protocol that proposes to apply an experiment-specific exponent to the correlation coefficients (WGCNA calls it “power”, which it is, but not in the context of the power law mentioned below) to strengthen the differences in the correlation data. Therefore, this power is chosen, for each experiment, just large enough so that in the derived correlation network, the fraction of genes that have *k*-many interactions with other genes is proportional to $k^{-\gamma}$ with γ being a small positive parameter. Networks with that property are called scale-free; the parameter γ describes how quickly this fraction gets smaller when the number of connections increases. Genes with a high number of connections are rare in scale-free networks, but they exist, and these “hub” genes are considered highly influential on the expression levels of genes in that module. Further, we filtered for modules that are associated with the health(span) phenotype (see next paragraph), and the hub genes are likely to also have a strong effect on this phenotype.

Only network modules whose WGCNA eigengene correlated with the “phenotypic health score” (p-value < 0.05) were retained further. Then, the 30 genes (see the WGCNA tutorial https://horvath.genetics.ucla.edu/html/CoexpressionNetwork/Rpackages/WGCNA/Tutorials/) most connected in a module according to the WGCNA *softConnectivity* function were considered for subsequent consensus analyses, and called “hub” genes hereafter. Besides

the modules, output of the WGCNA workflow is the topological overlap matrix with a quantitative description (termed *adjacency*) of all interactions between any pair of genes of an experiment. For each experiment, we determined a threshold at the 95% quantile of all the adjacency values. Only gene interactions with an adjacency above that experiment-wide threshold contribute to our analysis of interactions of genes in the health-associated modules. For the 30 hub genes, all pairwise interactions above that experiment-wide 95% quantile were thus exported. These interactions were then subjected to a pan-module search for consensus genes and consensus interactions, also across species by considering orthologs, presented in Tables 2 and 4. Orthologs were determined based on Ensembl version 101 (Yates *et al.*, 2019).

Further, for each health-associated module, the 30 genes correlating the strongest with the module's eigengene (reflecting average module behavior, also called "module membership" in WGCNA) were retrieved. Those found in at least two species are presented in Table 3. The correlation is taken in relation to the eigengene, and not in relation to the health phenotype score. Either would be fine for a ranking of the hub genes within a module, and the ranking is expected to be identical for the genes most central to a module. However, our particular interest was to abstract from the phenotypes of the experiment and thus utilize the WGCNA-performed modularization to influence the ranking. This is assumed to be particularly useful for experiments with multiple health-associated modules, each of which we expect to focus on a different aspect of health and for which hence also the genes should be ranked differently, to help analyzing that particular module most appropriately, and without any particularities pertaining to the health phenotype score. Multiple probesets describing the same gene, or its splice variants, were not distinguished and mapped to the same human gene, resulting in genes interacting with themselves. Such self-interactions were removed.

Network figures

The network figures were created with the R igraph package. A spring-embedding layout was chosen for the plots and manually refined. Figure 2 shows an overview on all hub genes from Table 2, their direct interactions and genes found in any species that connect to at least two hub genes. Additionally, Figures 2a-d in the Supplement were prepared separately for each species, i.e. they show only interactions from modules that WGCNA identified for an experiment based on samples from that species. Input to these supplement figures are the hub genes from Table 2 and all genes that are reachable from the hub genes which are no more than two transitions away. All interactions between the selected (reachable) genes were also added. The resulting graphs were simplified with the igraph minimum spanning tree implementation that maintains the connectivity of the graph but removes all redundant paths between genes. The spanning tree retains the stronger of two alternative paths between genes. A gene connected to a hub gene with a low adjacency value will thus lose that direct link if it is correlating strongly with another gene that has a strong correlation with that hub gene. Hub genes were determined from within WGCNA considering all interactions, not only the ones above the 95th percentile. Hub genes that are strongly connected for experiments in one species may not be equally dominating in another species. This and the competitive effect on directly connected hub genes (one cross-species, the other only observed for one species) imposed by the spanning tree give the impression that the

cross-species consensus hub genes are marginalized in Supplemental Figures 2a-d, albeit these graphs are seeded from the consensus hub genes and their interactions.

Results

We analysed all experiments listed in Table 1 with WGCNA. This analysis provided a modularization by an expression-based clustering of genes and allowed to describe the association of each module with the "health phenotype score". WGCNA also quantified the strength of gene correlations and determined hub genes for each module. We identified 12 genes (Table 2) that are among the 30 hub genes in health(span)-associated modules from at least two species. In total (Supplemental Table 1), 658 different genes were found among these top-30 hub genes of all modules as determined by WGCNA. An interaction network of the genes from Table 1, based on correlation of gene expression, is presented in Figure 2.

Table 2: Hub genes in health-associated WGCNA network modules, found in at least two species. *Orthologs were mapped to the human gene name using Ensembl. The human gene names also correspond to the names in mouse and rat, whereas the names of the orthologs in worms based on the Ensembl database are given in brackets.*

Gene human (worm)	Human	Mouse	Rat	Worm	Description in context of Healthspan
ACTN3 (atn-1)			x	x	Expressed in muscle, known marker for healthspan and athletes' muscle phenotypes (Pickering and Kiely, 2018). Localized to Z-discs, anchoring to actin filaments.
ANK1 (unc-44)		x		x	Ankyrin 1 (ANK1) is associated genetically with Diabetes type 2 (Spracklen *et al.*, 2020), spherocytosis (Qin *et al.*, 2020) and epigenetically with neurological diseases, likely triggered by ApoE with effect on TNFalpha and Akt (Morris *et al.*, 2018).
MRPL18 (mrpl-18)		x		x	The mitochondrial ribosomal protein L18 (MRPL18) is involved in the cytosolic stress response and promotes the translation of Hsp70 (Zhang *et al.*, 2015)
MYL1 (mlc-6 & mlc-5)	x		x		MYL1 encodes the myosin light chain 1 expressed in fast-twitch skeletal muscle fibers (Stuart *et al.*, 2016). Human ageing is associated with lower MYL1 content and higher MYL3 content (Cobley *et al.*, 2016).
PAXIP1 (pis-1)		x		x	The PAX interacting protein 1 (PAXIP1) contributes to DNA repair and correlates with breast cancer staging (De Gregoriis *et al.*, 2017).
PPP1CA (C06A1.3 & 26 others)	x			x	PPP1CA is one of three catalytic subunits of the serine/threonine specific protein phosphatase 1 (PP1), which is known to be involved in the regulation of glycogen metabolism, cell division, muscle contractility and protein synthesis (Ceuleman and Bollen, 2004). PPP1CA itself is linked to diverse tumor entities (Castro *et al.*, 2007, Sun *et al.*, 2019) and is involved in ERK/MAPK signaling (Sun *et al.*,

				2019), TGFβ signaling (Korrodi-Gregório *et al.*, 2014), Ras signaling and Ras-induced senescence (Ruiz *et al.*, 2008), spermatogenesis (Silva *et al.*, 2014) as well as in tau hyperphosphorylation leading to Alzheimer's disease (Banzhaf-Strathmann *et al.* 2014).
SCN3B (-)		x	x	The sodium voltage-gated channel beta subunit 3 (SCN3B) controls electrolytes and contributes to the pacemaking in the heart and has an effect on intracellular trafficking (Ishikawa *et al.*, 2012). It also suppresses senescence and apoptosis via its interaction with p53 and thus, is considered to be an oncogenic factor (Li *et al.*, 2020).
SDCBP (lin-10)		x		x Syntenin-1 (formerly Syndecan(SDC)-binding protein) regulates autophagy (Rajesh *et al.*, 2011) and together with Syndecan contributes to exosome formation (Baietti *et al.*, 2012) also in cancer cells (Fares *et al.*, 2017).
SKIV2L (skih-2)	x		x	The Ski2-like RNA helicase (SKIV2L) is part of the Super killer (SKI) complex and involved in mRNA degradation, DNA-RNA hybrid control, and telomere stability (Herrera-Moyano *et al.*, 2020). SKIV2L is also known to contribute to inflammatory bowel disease (Vardi *et al.*, 2018) and macular degeneration (Shuai *et al.*, 2017). Furthermore, SKIV2L features antiviral capacities and plays a role in innate immunity (Schott and Garcia-Blanco, 2020) associated with RNA exosomes (Eckard *et al.*, 2014).
TUBG1 (-)	x		x	TUBG1 encodes the tubulin gamma 1 protein, which, when mutated, can lead to brain malformations (Alvarado-Kristensson, 2018) with clinical features such as motor and intellectual disabilities and epilepsy. Moreover, TUBG1 is involved in tumor diseases, as shown for breast cancer (Blanco *et al.*, 2015), lung cancer (Maounis *et al.*, 2012) and medulloblastomas (Caracciolo *et al.*, 2010).
TYROBP (-)		x	x	The transmembrane immune signaling adaptor TYROBP is considered to be involved in Alzheimer's disease (Ma *et al.*, 2015; Pottier et al., 2016) and as a target of TERC in inflammatory processes (Liu *et al.*, 2019). In addition, TYROBP is suggested as a prognostic marker for gastric cancer and renal cell carcinoma (Wu *et al.*, 2020; Jiang *et al.*, 2020).
WIPF1 (wip-1)		x		x The WAS/WASL interacting protein family member 1 (WIPF1) regulates actin, phagocytosis, and neurotransmission and is among the top-3 genes upregulated by caloric restriction in the hypothalamus of wild-type mice (Stranahan *et al.*, 2012). Furthermore, overexpression of WIPF1, triggered by BRAF-mutation activated MAP kinase pathway, promotes aggressiveness of thyroid cancer and thus acts like an oncoprotein (Zhang *et al.*, 2017). Its oncoprotein character was also described for pancreatic

adenocarcinoma (Pan *et al.*, 2018) as well as breast cancer, glioma and colorectal cancer (Staub *et al.*, 2009).

Table 3: Genes correlating the strongest with the module's eigengene (quantifying module membership) in at least two species. *Genes in this table are among the top-30 of the module membership and found in experiments of at least two species. The gene name is marked in bold if that gene was listed as a hub gene in Table 2. The column "Consensus Correlation" flags "positive" (or "negative") to refer to an observed positive (or negative) correlation with the "health phenotype score" when the gene is upregulated. "mixed" indicates that the experiments did not yield a consensus direction of correlation. Supplement Table 1 extends this list to all genes that appear in the top 30 of modules of two or more experiments. The "#Experiments" column indicates the number of experiments with a module for which the gene was identified as a member.*

Gene		Consensus Correlation	#Experiments	Human	Mouse	Rat	Worm
AC068831.7	vps-33.2	*negative*	2		*negative*		*negative*
ADAM10	sup-17	*mixed*	2		*negative*		*positive*
APBB1IP	mig-10	*mixed*	2		*negative*		*positive*
CEBPB	cebp-1	*mixed*	2		*negative*	*positive*	
CREBBP	cbp-1	*negative*	3		*negative*		*negative*
EIF3F	eif-3.F	*positive*	2		*positive*		*positive*
INTS12	F53H1.4	*mixed*	2		*negative*		*positive*
KPNA3	ima-3	*mixed*	2		*negative*		*positive*
MEX3C	mex-3	*negative*	2	*negative*			*negative*
MRPL19	mrpl-19	*mixed*	2		*positive*		*negative*
MYL1	mlc-6	*positive*	2	*positive*		*positive*	
PAXIP1	pis-1	*positive*	2		*positive*		*positive*
PCNX2	B0511.12	*negative*	2		*negative*		*negative*
PPP1CA	C06A1.3	*mixed*	4	*positive*			*mixed*
PPP1CB	gsp-1	*positive*	2			*positive*	*positive*
PPP2R3C	-	*negative*	2	*negative*	*negative*		
RAB2A	unc-108	*negative*	2		*negative*		*negative*
RAB31	-	*negative*	2		*negative*	*negative*	
RPL29	rpl-29	*positive*	2		*positive*	*positive*	
RTN2	-	*mixed*	2	*positive*	*negative*		
RYR1	unc-68	*positive*	2	*positive*	*positive*		
SCN3B	-	*positive*	2		*positive*	*positive*	
SIX4	ceh-32	*negative*	2		*negative*		*negative*
SNRPD1	snr-3	*negative*	2		*negative*		*negative*

TMEM70	F32D8.5	*mixed*	2		*positive*		*negative*
TUBG1	-	*mixed*	2	*positive*	*negative*		
WIPF1	wip-1	*negative*	3		*negative*		*negative*
ZC3H15	F27D4.4	*negative*	2		*negative*		*negative*
SQSTM1	sqst-1	*negative*	3		*negative*	*negative*	*negative*

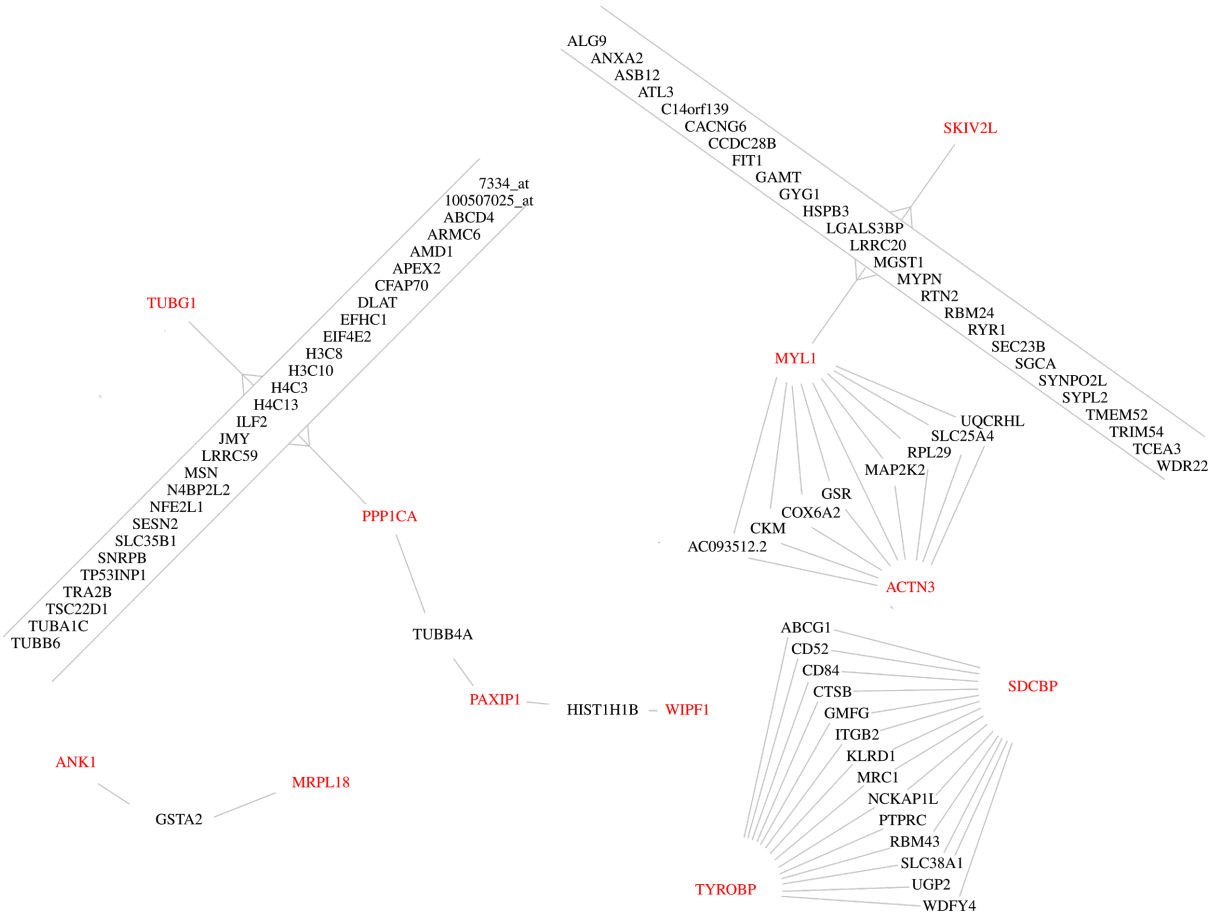

Figure 2: Cross-species conserved hub genes observed in health(span)-associated WGCNA modules, and genes that connect these hub genes*. Connections are interactions taken from the WGCNA adjacency matrix if the adjacency is above the 95th percentile of all interactions of that experiment and if for that experiment the interaction is in a health(span)-associated module. The only direct interaction between hub genes is between MYL1 and ACTN3.*

To prioritize the cross-species hub genes of Table 2, we also looked at the module membership of all genes for each module. The genes most correlating with the module's eigengene are reported and, analogous to Table 2, the genes that are found in multiple species were determined and listed in Table 3. This table further indicates whether a gene's change in expression is positively or negatively correlated with the eigengene of the WGCNA module to which it belongs, which in turn may be positively or negatively correlated with the health(span) phenotype. Supplement Table 1 shows the raw data that were used to

construct Table 3. To allow for a direct comparison of the genes' correlation with health(span), not quantitatively but in terms of direction (that is, up- or downregulation in relation to the health phenotype score), Table 3 presents a gene's inverted direction if the gene's module is already negatively correlated with the health(span) phenotype. The "Consensus Correlation" presents the direction that all experiments are in agreement with or "mixed" if the experiments differ in terms of their correlation with the health phenotype score. This information can be calculated for all genes, which we consider to help interpreting a module. For each module, the data for the 30 genes correlating the strongest with the module's eigengene are therefore provided in the supplement (Supplement Table 1).

Figure 3: Gene set enrichment analysis of cross-species hub genes for health(span) with g:profiler. *Input are genes from Table 2 that are observed in healthspan-associated modules of multiple species. Terms with a low coverage of genes are not suitable to describe the selection as a whole but may still direct the interpretation of parts of the network where these genes are connected.*

The intersection of Tables 2 (hub genes) and 3 (genes correlating with the health phenotype score) points to a subset of genes that are considered both influential and directly associated with health, i.e. MYL1, PAXIP1, PPP1CA, SCN3B, TUBG1 and WIPF1. The enrichment by g:profiler for the genes of Table 2 are shown in Figure 3. Supplement Figure 1a shows an enrichment analysis for the intersection of Tables 2 and 3 which is matching closely the enrichments in Figure 3, except that it does not feature the terms associated with muscle.

Supplement Figure 1b shows the enrichment for all genes in Table 3. The latter is the least robust since the enriched terms do not cover a large fraction of the genes as for the other enrichment analyses.

Discussion

Method

The onset of this investigation were all experiments in GEO/ArrayExpress that mention “healthspan” in their description (or “health” or “healthspan” in case of worm). For each experiment, from the descriptions that are provided for the samples in the database, a “health phenotype score” was derived. A gene expression correlation analysis with WGCNA yielded a gene coexpression network for each experiment as a set of modules of genes that correlate with the health(span) phenotype. We were interested in genes that are most connected, i.e. hub genes, for each module, and in their interactions as described by the WGCNA network. The correlation of genes with the module eigengene (Table 3), to predict a positive or negative association with health in the molecular context of that module, was only of secondary interest to us.

In this analysis, we focussed on common observations across two or more species and a variety of health-related phenotypes, including the reaction to drugs that extend healthspan (Table 1). The first steps of our analysis with WGCNA identified modules directly from the expression data, i.e. without inspecting a phenotype; the selection of health(span)-associated modules was performed in a later step. The WGCNA protocol was directly derived from the WGCNA tutorial.

The selection of genes, based on strong connectivity, from modules selected in such a way shall hence be considered robust even if the mapping of the multi-factorial sample descriptions to a single factor, that is, the health phenotype score describing the health-effect observed in samples, may allow for plausible alternatives. This is another reason, besides the need for abstraction to compare experiments, why we consider it advantageous to compare the module’s genes against the module’s eigengene, which is derived solely by an inspection of the expression data, and not against the health phenotype score (as done in Table 3). The manual intervention to derive the health phenotype score was solely needed to filter for health(span) associated modules (Table 3).

To filter for gene interactions, we decided to filter for the strongest 5% of adjacencies from each experiment, further constrained to modules that are associated with the health(span) phenotype score; see the Methods section for details. This experiment-dependent threshold reflects that experiments differ in the number of samples and subgroups and hence in the contrasts to separate genes by their correlations.

The authors of WGCNA suggested that their software can be used to perform network meta-studies from multiple microarray experiments in a single WGCNA setup (Langfelder *et al.*, 2013). But they clearly stated that the same module needs to be robust across experiments to directly perform WGCNA on a single joint matrix based on all expression data. For the very diverse set of experiments contributing to our analysis and their polygenic phenotype this is not necessarily expected to be the case, i.e. experiments may have their

true healthspan-associated module in different sections of the transcriptome. Indeed, we did not observe any interactions to have orthologs across species. The setup presented here is pragmatic and robust, i.e. individual experiments can be removed without affecting the gene interactions determined for another experiment. Of major concern for us was that hub genes are expected to show a measurable effect on health(span) only under the conditions of those ArrayExpress/GEO experiments in which they are differentially expressed. To follow this work up with wet lab confirmations, it is hence essential to provide provenance information on how the change to the hub gene's expression was induced, i.e. a pointer to the ArrayExpress/GEO experiment. In a joint matrix across many experiments this information would be more difficult to retrieve, which suggests not to conduct the integration of experiments directly within a single WCGNA analysis.

Furthermore, for integrating interaction data from multiple experiments, the authors of WGCNA suggested to weigh the interactions from each experiment to derive a single joint adjacency matrix and they suggested to apply a threshold on that single matrix to derive a network. Because of the heterogeneity of our experiments, we cannot tell which experiment would be more informative for health(span), compared to another, and thus could not adjust weights accordingly. By treating all experiments individually, and the null hypothesis that all experiments have the same fraction of true interactions that shall be identified by the respective highest adjacency values, we could use an experiment-tailored threshold for filtering the interactions. Therefore, we used the 95th percentile of correlation values in the adjacency matrix, for each experiment, to adapt the selection of the interactions to be forwarded to describe a meta-study consensus (see Figures 1 and 2). These gene interactions may be trusted and they thus could be reassembled into a larger integrated meta-study network to reflect the molecular neighborhoods of hub genes, which we presented as Figure 2 (cross-species) and Supplement Figures 2a-d (for multiple modules of the respective same species). The comparison of findings across species further strengthens the confidence in the WGCNA results. Thus, we identified conserved candidate regulators of health(span).

An important technical concern lies with the interpretation of gene expression correlation data for RNA-seq experiments, which have an intrinsic high noise-level for low-abundant genes. We have recently shown (Struckmann *et al.*, 2020) that even for array data (that are less noisy for low-abundant genes), also the low-abundant genes have a measurable effect on a ranking of genes by Pearson correlation, and this is likely also the case for module calculations as performed here. This concern has to be borne in mind in the following interpretation of the modules in terms of biological functionality.

Cross-species hub genes and their interactions

Most of the hub genes identified by our analysis (Table 2) have been described in a health(span)-context before. The gene set enrichment analysis with g:profiler describes the molecular roles of the cross-species hub genes (Table 2) as specifically associated with a) features of the muscle and b) actin filament-based organelles and movement (Figure 3). The worm is a model species also for muscle development because of striking similarities of its muscles to mammalian muscle tissue (Christian and Benian, 2020), and movement (locomotion) is an important phenotype in all species towards operationalizing health by

quantification (Fuellen *et al.* 2019). For human, rat and mouse in Table 1, there are experiments for which samples were selectively taken from muscle tissue, but not so for the worm, which is routinely sequenced as a whole. Upon closer inspection of the enrichment results of Figure 3, we found that “actin filament-based movement” refers to a wide spectrum of processes, i.e. genes that support actin polymerisation (WIPF1), the motor protein myosin (MYL1) or the transition of endosomes into exosomes for intercellular communication (SDCBP).

The number of experiments of vertebrates and invertebrates is balanced. Apart from a lack of tissue specificity, the experiments for the worm differ from rodents and humans, in that experiments for the worm may comprise samples from different larval stages. This may ease the task to find strong correlations between genes, but specificity for aging-associated processes is likely reduced.

Inspecting the distribution of hub genes by species, we found no more than five of the 12 hub genes in worm, cf. Supplement Figure 2b, and four in human, cf. Supplement Figure 2a. The only conserved direct interaction between consensus hub genes was observed between MYL1 and ACTN3 (Figure 2). However, interactions were found multiple times for experiments of the same species, namely ABRA with VRK2, AQP11 with GSTA2 and CYLD with PCNX2 for the worm. These three interactions are shown in Supplement Figure 2b and the VRK2 gene remains directly connected with the PPP1CA hub gene also after the minimum-spanning-tree-based edge removal. VRK2 is described to have downstream effects on the consensus hub gene PPP1CA (Cossa *et al.*, 2020) via GSK3beta (Lee *et al.*, 2016). Its genetic variants are associated with a series of neurological diseases and viral infection, but also with healthspan associated sleep patterns (Dashti *et al.*, 2019). The interactions conserved in multiple species are not confirmed in STRING (Szklarczyk *et al.*, 2021) for the human, but for the worm, the consensus hub gene PPP1CA (C06A1.3) links to VRK2 (tag-191).

By interpreting the enrichments in Supplement Figure 3 we can gain more insight into how the genes we discovered may be involved in health. An example is the enrichment referring to the TYROBP pathway described in wikipathways and to the GO term Leukocyte activation (Supplement Figure 3a). Genes connecting MYL1 and SKIV2L are involved in muscular structures (Supplement Figure 3b). Tubulins (e.g. TUBG1) are known to bind to PP1, of which PPP1CA is a subunit and together these proteins regulate histone acetylation (Ding *et al.*, 2008), which is reflected by the genes connecting PPP1CA and TUBG1 (Supplement Figure 3c). Further, enhanced histone acetylation is associated with extended health and lifespan in worm (Zhang *et al.*, 2009).

The highly connected genes selected in this study differ from the list we recently published (Möller *et al.*, 2020). This WGCNA-based study does not refer to prior knowledge about genetic contributions and does not perform a factor analysis to directly associate genes with a health(span) phenotype. Instead, our focus here is the network-centric interpretation of correlations within gene co-expression clusters, i.e. WCGNA modules. It is the module as a whole that correlates in its expression with health, not necessarily the individual genes. Table 3 lists genes within the clusters that are most representative for the features/characteristics of the cluster in question, i.e. that have the highest degree of *module membership* by

WGCNA definition, and in the table, there are marks (by boldface) for the subset of genes that are also hub genes. Of the cross-species hub genes in Table 2, six are also listed in Table 3. Others are “near misses”, e.g. Table 3 does not list the consensus hub gene MRPL18 but MRPL19. And besides the consensus hub gene PPP1CA, other PP1 subunits like PPP1CB and PPP2R3C are found in two species (Table 3). PPP1CB was also found as a hub gene, but only for the worm.

In Table 3, we report SQSTM1 as the only gene that is associated with health in three species. That gene was long suggested to be aging- and health-related (Bitto *et al.*, 2014; Sánchez-Martín and Komatsu, 2018), also for human, even though it was only found associated in the analyses of the animal experiments in this study. Its transcript is negatively correlated with health, but SQSTM1 overexpression is known to extend healthspan in worm (Kumsta *et al.*, 2019), which may be suggestive for a protective upregulation effect.

Overall, our meta-analysis of a very diverse set of transcriptomics experiments successfully identified genes which, for the most part, were already established to be closely associated with health(span), and together they have a strong and meaningful GO term enrichment. The enrichment of muscle-related genes can be credited to our focus on health(span) experiments, and our study found many “actin filament-based movement” genes (Figure 3) that provide the cellular infrastructure not just for movement, but also for signalling and cell division, which may be triggered/blocked whenever cells start to feel unwell. If so, then it may be possible to detect many healthspan genes solely by inspecting cellular data. This hypothesis may be confirmed by an extension of our setup to a larger set of cellular transcriptomics data sets for which samples vary in their genetic or environmental exposure to stress factors.

This study provided a cross-species meta-study of gene interactions for health(span)-related datasets in ArrayExpress/GEO. It focused on a co-expression network analysis and subsequently on derived hub genes, instead of a focus on those genes that correlate the most with the healthspan phenotype score. This approach shall allow for an abstraction from the experiment at hand and permit a search for common mediators of an effect. The proposed consensus hub genes were plausible in their implication into health(span). Their interactions could be confirmed in STRING, or were found consistent with gene set enrichment analyses and they may support the interpretation of joint or epistatic effects between pairs of haplotypes in healthspan GWAS or linkage analyses. The protocol as provided with WGCNA is very transparent so that findings can be traced back to the experiments that are backing them, to serve as a template for further investigations in the wet lab.

Acknowledgements

This work was supported by a project from the European Union’s Horizon 2020 research and innovation programme under Grant agreement No 633589 (Aging with Elegans), and by the BMBF (Validierung des technologischen und gesellschaftlichen Innovationspotenzials wissenschaftlicher Forschung – VIP+, FKZ: 03VP06230).

Availability

Our implementation is available online at https://bitbucket.org/ibima/healthspantranscriptomicsnetworks/.

References

Adler, Priit, Raivo Kolde, Meelis Kull, Aleksandr Tkachenko, Hedi Peterson, Jüri Reimand, and Jaak Vilo. 2009. “Mining for Coexpression across Hundreds of Datasets Using Novel Rank Aggregation and Visualization Methods.” *Genome Biology* 10 (12): R139. https://doi.org/10.1186/gb-2009-10-12-r139.

Aging Atlas Consortium, Guang-Hui Liu, Yiming Bao, Jing Qu, Weiqi Zhang, Tao Zhang, Wang Kang, et al. 2021. “Aging Atlas: A Multi-Omics Database for Aging Biology.” *Nucleic Acids Research* 49 (D1): D825–30. https://doi.org/10.1093/nar/gkaa894.

Alvarado-Kristensson, Maria. 2018. “γ-Tubulin as a Signal-Transducing Molecule and Meshwork with Therapeutic Potential.” *Signal Transduction and Targeted Therapy* 3 (1): 24. https://doi.org/10.1038/s41392-018-0021-x.

Amar, David, Hershel Safer, and Ron Shamir. 2013. “Dissection of Regulatory Networks That Are Altered in Disease via Differential Co-Expression.” Edited by Donna K. Slonim. *PLoS Computational Biology* 9 (3): e1002955. https://doi.org/10.1371/journal.pcbi.1002955.

Athar, Awais, Anja Füllgrabe, Nancy George, Haider Iqbal, Laura Huerta, Ahmed Ali, Catherine Snow, et al. 2019. “ArrayExpress Update – from Bulk to Single-Cell Expression Data.” *Nucleic Acids Research* 47 (D1): D711–15. https://doi.org/10.1093/nar/gky964.

Avelar, Roberto A., Javier Gómez Ortega, Robi Tacutu, Eleanor J. Tyler, Dominic Bennett, Paolo Binetti, Arie Budovsky, et al. 2020. “A Multidimensional Systems Biology Analysis of Cellular Senescence in Aging and Disease.” *Genome Biology* 21 (1): 91. https://doi.org/10.1186/s13059-020-01990-9.

Baietti, Maria Francesca, Zhe Zhang, Eva Mortier, Aurélie Melchior, Gisèle Degeest, Annelies Geeraerts, Ylva Ivarsson, et al. 2012. “Syndecan-Syntenin-ALIX Regulates the Biogenesis of Exosomes.” *Nature Cell Biology* 14 (7): 677–85. https://doi.org/10.1038/ncb2502.

Banzhaf-Strathmann, Julia, Eva Benito, Stephanie May, Thomas Arzberger, Sabina Tahirovic, Hans Kretzschmar, André Fischer, and Dieter Edbauer. 2014. “Micro RNA -125b Induces Tau Hyperphosphorylation and Cognitive Deficits in Alzheimer’s Disease.” *The EMBO Journal* 33 (15): 1667–80. https://doi.org/10.15252/embj.201387576.

Bitto, Alessandro, Chad A. Lerner, Timothy Nacarelli, Elizabeth Crowe, Claudio Torres, and Christian Sell. 2014. “P62/SQSTM1 at the Interface of Aging, Autophagy, and Disease.” *AGE* 36 (3): 9626. https://doi.org/10.1007/s11357-014-9626-3.

Blanco, Ignacio, Karoline Kuchenbaecker, Daniel Cuadras, Xianshu Wang, Daniel Barrowdale, Gorka Ruiz de Garibay, Pablo Librado, et al. 2015. “Assessing Associations between the AURKA-HMMR-TPX2-TUBG1 Functional Module and Breast Cancer Risk in BRCA1/2 Mutation Carriers.” *PloS One* 10 (4): e0120020. https://doi.org/10.1371/journal.pone.0120020.

Brewer, Rachel A., Victoria K. Gibbs, and Daniel L. Smith. 2016. “Targeting Glucose Metabolism for Healthy Aging.” *Nutrition and Healthy Aging* 4 (1): 31–46. https://doi.org/10.3233/NHA-160007.

Bushnell, Brian, Jonathan Rood, and Esther Singer. 2017. “BBMerge – Accurate Paired Shotgun Read Merging via Overlap.” Edited by Patrick Jon Biggs. *PLOS ONE* 12 (10): e0185056. https://doi.org/10.1371/journal.pone.0185056.

Caracciolo, Valentina, Luca D’Agostino, Eduarda Dráberová, Vladimíra Sládková, Catena Crozier-Fitzgerald, Dimitri P. Agamanolis, Jean-Pierre de Chadarévian, et al. 2010. “Differential Expression and Cellular Distribution of Gamma-Tubulin and BetaIII-Tubulin in Medulloblastomas and Human Medulloblastoma Cell Lines.” *Journal of Cellular Physiology* 223 (2): 519–29. https://doi.org/10.1002/jcp.22077.

Castermans, Dries, Ils Somers, Johan Kriel, Wendy Louwet, Stefaan Wera, Matthias Versele, Veerle Janssens, and Johan M Thevelein. 2012. "Glucose-Induced Posttranslational Activation of Protein Phosphatases PP2A and PP1 in Yeast." *Cell Research* 22 (6): 1058–77. https://doi.org/10.1038/cr.2012.20.

Castro, M. E., I. Ferrer, A. Cascon, M. V. Guijarro, M. Lleonart, S. R. y Cajal, J. F.M. Leal, M. Robledo, and A. Carnero. 2007. "PPP1CA Contributes to the Senescence Program Induced by Oncogenic Ras." *Carcinogenesis* 29 (3): 491–99. https://doi.org/10.1093/carcin/bgm246.

Ceulemans, Hugo, and Mathieu Bollen. 2004. "Functional Diversity of Protein Phosphatase-1, a Cellular Economizer and Reset Button." *Physiological Reviews* 84 (1): 1–39. https://doi.org/10.1152/physrev.00013.2003.

Chen, Di, Patrick Wai-Lun Li, Benjamin A. Goldstein, Waijiao Cai, Emma Lynn Thomas, Fen Chen, Alan E. Hubbard, Simon Melov, and Pankaj Kapahi. 2013. "Germline Signaling Mediates the Synergistically Prolonged Longevity Produced by Double Mutations in Daf-2 and Rsks-1 in C. Elegans." *Cell Reports* 5 (6): 1600–1610. https://doi.org/10.1016/j.celrep.2013.11.018.

Christian, Courtney J., and Guy M. Benian. 2020. "Animal Models of Sarcopenia." *Aging Cell* 19 (10). https://doi.org/10.1111/acel.13223.

Clough, Emily, and Tanya Barrett. 2016. "The Gene Expression Omnibus Database." In *Statistical Genomics*, edited by Ewy Mathé and Sean Davis, 1418:93–110. Methods in Molecular Biology. New York, NY: Springer New York. https://doi.org/10.1007/978-1-4939-3578-9_5.

Cobley, James, Zulezwan Ab. Malik, James Morton, Graeme Close, Ben Edwards, and Jatin Burniston. 2016. "Age- and Activity-Related Differences in the Abundance of Myosin Essential and Regulatory Light Chains in Human Muscle." *Proteomes* 4 (2): 15. https://doi.org/10.3390/proteomes4020015.

Cossa, Giacomo, Isabelle Roeschert, Florian Prinz, Apoorva Baluapuri, Raphael Silveira Vidal, Christina Schülein-Völk, Yun-Chien Chang, et al. 2020. "Localized Inhibition of Protein Phosphatase 1 by NUAK1 Promotes Spliceosome Activity and Reveals a MYC-Sensitive Feedback Control of Transcription." *Molecular Cell* 77 (6): 1322-1339.e11. https://doi.org/10.1016/j.molcel.2020.01.008.

Cowen, Lenore, Trey Ideker, Benjamin J. Raphael, and Roded Sharan. 2017. "Network Propagation: A Universal Amplifier of Genetic Associations." *Nature Reviews Genetics* 18 (9): 551–62. https://doi.org/10.1038/nrg.2017.38.

Dam, Sipko van, Rui Cordeiro, Thomas Craig, Jesse van Dam, Shona H Wood, and João de Magalhães. 2012. "GeneFriends: An Online Co-Expression Analysis Tool to Identify Novel Gene Targets for Aging and Complex Diseases." *BMC Genomics* 13 (1): 535. https://doi.org/10.1186/1471-2164-13-535.

Dam, Sipko van, Urmo Võsa, Adriaan van der Graaf, Lude Franke, and João Pedro de Magalhães. 2017. "Gene Co-Expression Analysis for Functional Classification and Gene–Disease Predictions." *Briefings in Bioinformatics*, January, bbw139. https://doi.org/10.1093/bib/bbw139.

Dashti, Hassan S., Samuel E. Jones, Andrew R. Wood, Jacqueline M. Lane, Vincent T. van Hees, Heming Wang, Jessica A. Rhodes, et al. 2019. "Genome-Wide Association Study Identifies Genetic Loci for Self-Reported Habitual Sleep Duration Supported by Accelerometer-Derived Estimates." *Nature Communications* 10 (1): 1100. https://doi.org/10.1038/s41467-019-08917-4.

Del Puerto-Nevado, Laura, Aranzazu Santiago-Hernandez, Sonia Solanes-Casado, Nieves Gonzalez, Marta Ricote, Marta Corton, Isabel Prieto, et al. 2019. "Diabetes-mediated Promotion of Colon Mucosa Carcinogenesis Is Associated with Mitochondrial Dysfunction." *Molecular Oncology* 13 (9): 1887–97. https://doi.org/10.1002/1878-0261.12531.

Ding, Huiping, Philip J. Dolan, and Gail V. W. Johnson. 2008. "Histone Deacetylase 6 Interacts with the Microtubule-Associated Protein Tau." *Journal of Neurochemistry* 106 (5): 2119–30. https://doi.org/10.1111/j.1471-4159.2008.05564.x.

Dobin, Alexander, Carrie A. Davis, Felix Schlesinger, Jorg Drenkow, Chris Zaleski, Sonali Jha, Philippe Batut, Mark Chaisson, and Thomas R. Gingeras. 2013. "STAR: Ultrafast Universal RNA-Seq Aligner." *Bioinformatics* 29 (1): 15–21. https://doi.org/10.1093/bioinformatics/bts635.

Dönertaş, Handan Melike, Matías Fuentealba Valenzuela, Linda Partridge, and Janet M. Thornton.

2018. “Gene Expression-Based Drug Repurposing to Target Aging.” *Aging Cell* 17 (5): e12819. https://doi.org/10.1111/acel.12819.

Eckard, Sterling C, Gillian I Rice, Alexandre Fabre, Catherine Badens, Elizabeth E Gray, Jane L Hartley, Yanick J Crow, and Daniel B Stetson. 2014. “The SKIV2L RNA Exosome Limits Activation of the RIG-I-like Receptors.” *Nature Immunology* 15 (9): 839–45. https://doi.org/10.1038/ni.2948.

Fares, Joanna, Rudra Kashyap, and Pascale Zimmermann. 2017. “Syntenin: Key Player in Cancer Exosome Biogenesis and Uptake?” *Cell Adhesion & Migration* 11 (2): 124–26. https://doi.org/10.1080/19336918.2016.1225632.

Finley, L. W. S., J. Lee, A. Souza, V. Desquiret-Dumas, K. Bullock, G. C. Rowe, V. Procaccio, C. B. Clish, Z. Arany, and M. C. Haigis. 2012. “Skeletal Muscle Transcriptional Coactivator PGC-1 Mediates Mitochondrial, but Not Metabolic, Changes during Calorie Restriction.” *Proceedings of the National Academy of Sciences* 109 (8): 2931–36. https://doi.org/10.1073/pnas.1115813109.

Franz, Max, Harold Rodriguez, Christian Lopes, Khalid Zuberi, Jason Montojo, Gary D Bader, and Quaid Morris. 2018. “GeneMANIA Update 2018.” *Nucleic Acids Research* 46 (W1): W60–64. https://doi.org/10.1093/nar/gky311.

Fuellen, Georg, Ludger Jansen, Alan A Cohen, Walter Luyten, Manfred Gogol, Andreas Simm, Nadine Saul, et al. 2019. “Health and Aging: Unifying Concepts, Scores, Biomarkers and Pathways.” *Aging and Disease* 10 (4): 883. https://doi.org/10.14336/AD.2018.1030.

Greer, Eric L., Travis J. Maures, Anna G. Hauswirth, Erin M. Green, Dena S. Leeman, Géraldine S. Maro, Shuo Han, Max R. Banko, Or Gozani, and Anne Brunet. 2010. “Members of the H3K4 Trimethylation Complex Regulate Lifespan in a Germline-Dependent Manner in C. Elegans.” *Nature* 466 (7304): 383–87. https://doi.org/10.1038/nature09195.

Harvey, Simon C, Gary LA Barker, Alison Shorto, and Mark E Viney. 2009a. “Natural Variation in Gene Expression in the Early Development of Dauer Larvae of Caenorhabditis Elegans.” *BMC Genomics* 10 (1): 325. https://doi.org/10.1186/1471-2164-10-325.

Herrera-Moyano, Emilia, Rosa Maria Porreca, Lepakshi Ranjha, Roser Gonzalez-Franco, Eleni Skourti, Ying Sun, Emmanouil Stylianakis, Alex Montoya, Holger Kramer, and Jean-Baptiste Vannier. 2020. “Human SKI Is a Telomere-Associated Complex Involved in DNA-RNA Hybrid Control and Telomere Stability.” Preprint. Molecular Biology. https://doi.org/10.1101/2020.05.20.107144.

Ideker, Trey, Janusz Dutkowski, and Leroy Hood. 2011. “Boosting Signal-to-Noise in Complex Biology: Prior Knowledge Is Power.” *Cell* 144 (6): 860–63. https://doi.org/10.1016/j.cell.2011.03.007.

Ishikawa, Taisuke, Naohiko Takahashi, Seiko Ohno, Harumizu Sakurada, Kazufumi Nakamura, Young Keun On, Jeong Euy Park, et al. 2013. “Novel SCN3B Mutation Associated with Brugada Syndrome Affects Intracellular Trafficking and Function of Nav1.5.” *Circulation Journal: Official Journal of the Japanese Circulation Society* 77 (4): 959–67. https://doi.org/10.1253/circj.cj-12-0995.

Jackson, Belinda M., Patricia Abete-Luzi, Michael W. Krause, and David M. Eisenmann. 2014. “Use of an Activated Beta-Catenin to Identify Wnt Pathway Target Genes in *Caenorhabditis Elegans* , Including a Subset of Collagen Genes Expressed in Late Larval Development.” *G3: Genes|Genomes|Genetics* 4 (4): 733–47. https://doi.org/10.1534/g3.113.009522.

Jiang, Junjie, Yongfeng Ding, Mengjie Wu, Xiadong Lyu, Haifeng Wang, Yanyan Chen, Haiyong Wang, and Lisong Teng. 2020. “Identification of TYROBP and C1QB as Two Novel Key Genes With Prognostic Value in Gastric Cancer by Network Analysis.” *Frontiers in Oncology* 10 (September): 1765. https://doi.org/10.3389/fonc.2020.01765.

Kim, Yeo Jin, Hyun Soo Kim, and Young Rok Seo. 2018. “Genomic Approach to Understand the Association of DNA Repair with Longevity and Healthy Aging Using Genomic Databases of Oldest-Old Population.” *Oxidative Medicine and Cellular Longevity* 2018: 1–12. https://doi.org/10.1155/2018/2984730.

Korrodi-Gregório, Luís, Joana Vieira Silva, Luís Santos-Sousa, Maria João Freitas, Juliana Felgueiras, and Margarida Fardilha. 2014. “TGF-β Cascade Regulation by PPP1 and Its Interactors -Impact on Prostate Cancer Development and

Therapy." *Journal of Cellular and Molecular Medicine* 18 (4): 555–67. https://doi.org/10.1111/jcmm.12266.

Kotlyar, Max, Chiara Pastrello, Zara Malik, and Igor Jurisica. 2019. "IID 2018 Update: Context-Specific Physical Protein–Protein Interactions in Human, Model Organisms and Domesticated Species." *Nucleic Acids Research* 47 (D1): D581–89. https://doi.org/10.1093/nar/gky1037.

Kucera, Mike, Ruth Isserlin, Arkady Arkhangorodsky, and Gary D. Bader. 2016. "AutoAnnotate: A Cytoscape App for Summarizing Networks with Semantic Annotations." *F1000Research* 5 (July): 1717. https://doi.org/10.12688/f1000research.9090.1.

Kumsta, Caroline, Jessica T. Chang, Reina Lee, Ee Phie Tan, Yongzhi Yang, Rute Loureiro, Elizabeth H. Choy, et al. 2019. "The Autophagy Receptor P62/SQST-1 Promotes Proteostasis and Longevity in C. Elegans by Inducing Autophagy." *Nature Communications* 10 (1): 5648. https://doi.org/10.1038/s41467-019-13540-4.

Langfelder, Peter, and Steve Horvath. 2008. "WGCNA: An R Package for Weighted Correlation Network Analysis." *BMC Bioinformatics* 9 (1): 559. https://doi.org/10.1186/1471-2105-9-559.

Langfelder, Peter, Paul S. Mischel, and Steve Horvath. 2013. "When Is Hub Gene Selection Better than Standard Meta-Analysis?" Edited by Timothy Ravasi. *PLoS ONE* 8 (4): e61505. https://doi.org/10.1371/journal.pone.0061505.

Lee, Eunju, Hye Guk Ryu, Sangjune Kim, Dohyun Lee, Young-Hun Jeong, and Kyong-Tai Kim. 2016. "Glycogen Synthase Kinase 3β Suppresses Polyglutamine Aggregation by Inhibiting Vaccinia-Related Kinase 2 Activity." *Scientific Reports* 6 (1): 29097. https://doi.org/10.1038/srep29097.

Lee, John, Manthan Shah, Sara Ballouz, Megan Crow, and Jesse Gillis. 2020. "CoCoCoNet: Conserved and Comparative Co-Expression across a Diverse Set of Species." *Nucleic Acids Research* 48 (W1): W566–71. https://doi.org/10.1093/nar/gkaa348.

Lehrbach, N. J., C. Castro, K. J. Murfitt, C. Abreu-Goodger, J. L. Griffin, and E. A. Miska. 2012. "Post-Developmental MicroRNA Expression Is Required for Normal Physiology, and Regulates Aging in Parallel to Insulin/IGF-1 Signaling in C. Elegans." *RNA* 18 (12): 2220–35. https://doi.org/10.1261/rna.035402.112.

Leinonen, R., R. Akhtar, E. Birney, L. Bower, A. Cerdeno-Tarraga, Y. Cheng, I. Cleland, et al. 2011. "The European Nucleotide Archive." *Nucleic Acids Research* 39 (Database): D28–31. https://doi.org/10.1093/nar/gkq967.

Leiserson, Mark DM, Jonathan V Eldridge, Sohini Ramachandran, and Benjamin J Raphael. 2013. "Network Analysis of GWAS Data." *Current Opinion in Genetics & Development* 23 (6): 602–10. https://doi.org/10.1016/j.gde.2013.09.003.

Li, Bo, Victor Ruotti, Ron M. Stewart, James A. Thomson, and Colin N. Dewey. 2010. "RNA-Seq Gene Expression Estimation with Read Mapping Uncertainty." *Bioinformatics* 26 (4): 493–500. https://doi.org/10.1093/bioinformatics/btp692.

Li, Ming-Li, Shi-Hao Wu, Jin-Jin Zhang, Hang-Yu Tian, Yong Shao, Zheng-Bo Wang, David M. Irwin, Jia-Li Li, Xin-Tian Hu, and Dong-Dong Wu. 2019. "547 Transcriptomes from 44 Brain Areas Reveal Features of the Aging Brain in Non-Human Primates." *Genome Biology* 20 (1): 258. https://doi.org/10.1186/s13059-019-1866-1.

Li, Shuai, Jiadi Han, Guili Guo, Yudi Sun, Tingting Zhang, Mingyi Zhao, Yijia Xu, Yong Cui, Yanfeng Liu, and Jinghai Zhang. 2020. "Voltage-Gated Sodium Channels B3 Subunit Promotes Tumorigenesis in Hepatocellular Carcinoma by Facilitating P53 Degradation." *FEBS Letters* 594 (3): 497–508. https://doi.org/10.1002/1873-3468.13641.

Liang, Yaru, and Zhao Wang. 2018. "Which Is the Most Reasonable Anti-Aging Strategy: Meta-Analysis." In *Aging and Aging-Related Diseases*, edited by Zhao Wang, 1086:267–82. Advances in Experimental Medicine and Biology. Singapore: Springer Singapore. https://doi.org/10.1007/978-981-13-1117-8_17.

Liu, Haiying, Yiding Yang, Yuanlong Ge, Juanhong Liu, and Yong Zhao. 2019. "TERC Promotes Cellular Inflammatory Response Independent of Telomerase." *Nucleic Acids Research* 47 (15): 8084–95. https://doi.org/10.1093/nar/gkz584.

Ma, Jing, Teng Jiang, Lan Tan, and Jin-Tai Yu. 2015. "TYROBP in Alzheimer's Disease." *Molecular Neurobiology* 51 (2): 820–26. https://doi.org/10.1007/s12035-014-8811-9.

Magalhães, João Pedro de, João Curado, and George M. Church. 2009. "Meta-Analysis of Age-Related Gene Expression Profiles Identifies Common Signatures of Aging." *Bioinformatics* 25 (7): 875–81. https://doi.org/10.1093/bioinformatics/btp073.

Magger, Oded, Yedael Y. Waldman, Eytan Ruppin, and Roded Sharan. 2012. "Enhancing the Prioritization of Disease-Causing Genes through Tissue Specific Protein Interaction Networks." Edited by Donna K. Slonim. *PLoS Computational Biology* 8 (9): e1002690. https://doi.org/10.1371/journal.pcbi.1002690.

Manole, Andreea, Stephanie Efthymiou, Emer O'Connor, Marisa I. Mendes, Matthew Jennings, Reza Maroofian, Indran Davagnanam, et al. 2020. "De Novo and Bi-Allelic Pathogenic Variants in NARS1 Cause Neurodevelopmental Delay Due to Toxic Gain-of-Function and Partial Loss-of-Function Effects." *The American Journal of Human Genetics* 107 (2): 311–24. https://doi.org/10.1016/j.ajhg.2020.06.016.

Maounis, Nicoletta F., Eduarda Dráberová, Eleni Mahera, Maria Chorti, Valentina Caracciolo, Tetyana Sulimenko, Dimitra Riga, et al. 2012. "Overexpression of γ-Tubulin in Non-Small Cell Lung Cancer." *Histology and Histopathology* 27 (9): 1183–94. https://doi.org/10.14670/HH-27.1183.

Mercken, Evi M., Seth D. Crosby, Dudley W. Lamming, Lellean JeBailey, Susan Krzysik-Walker, Dennis T. Villareal, Miriam Capri, et al. 2013. "Calorie Restriction in Humans Inhibits the PI3K/AKT Pathway and Induces a Younger Transcription Profile." *Aging Cell* 12 (4): 645–51. https://doi.org/10.1111/acel.12088.

Mercken, Evi M., Sarah J. Mitchell, Alejandro Martin-Montalvo, Robin K. Minor, Maria Almeida, Ana P. Gomes, Morten Scheibye-Knudsen, et al. 2014. "SRT2104 Extends Survival of Male Mice on a Standard Diet and Preserves Bone and Muscle Mass." *Aging Cell* 13 (5): 787–96. https://doi.org/10.1111/acel.12220.

Möller, Steffen, Nadine Saul, Alan A. Cohen, Rüdiger Köhling, Sina Sender, Hugo Murua Escobar, Christian Junghanss, et al. 2020. "Healthspan Pathway Maps in C. Elegans and Humans Highlight Transcription, Proliferation/Biosynthesis and Lipids." *Aging* 12 (13): 12534–81. https://doi.org/10.18632/aging.103514.

Morris, Gerwyn, Michael Berk, Michael Maes, and Basant K. Puri. 2019. "Could Alzheimer's Disease Originate in the Periphery and If So How So?" *Molecular Neurobiology* 56 (1): 406–34. https://doi.org/10.1007/s12035-018-1092-y.

Obayashi, Takeshi, Yuki Kagaya, Yuichi Aoki, Shu Tadaka, and Kengo Kinoshita. 2019. "COXPRESdb v7: A Gene Coexpression Database for 11 Animal Species Supported by 23 Coexpression Platforms for Technical Evaluation and Evolutionary Inference." *Nucleic Acids Research* 47 (D1): D55–62. https://doi.org/10.1093/nar/gky1155.

Pan, Yu, Fengchun Lu, Ping Xiong, Maoen Pan, Zheyang Zhang, Xianchao Lin, Minggui Pan, and Heguang Huang. 2018. "WIPF1 Antagonizes the Tumor Suppressive Effect of MiR-141/200c and Is Associated with Poor Survival in Patients with PDAC." *Journal of Experimental & Clinical Cancer Research* 37 (1): 167. https://doi.org/10.1186/s13046-018-0848-6.

Pickering, Craig, and John Kiely. 2018. "ACTN3, Morbidity, and Healthy Aging." *Frontiers in Genetics* 9 (January): 15. https://doi.org/10.3389/fgene.2018.00015.

Pottier, Cyril, Thomas A. Ravenscroft, Patricia H. Brown, NiCole A. Finch, Matt Baker, Meeia Parsons, Yan W. Asmann, et al. 2016. "TYROBP Genetic Variants in Early-Onset Alzheimer's Disease." *Neurobiology of Aging* 48 (December): 222.e9-222.e15. https://doi.org/10.1016/j.neurobiolaging.2016.07.02.

Pujol, Nathalie, Olivier Zugasti, Daniel Wong, Carole Couillault, C. Léopold Kurz, Hinrich Schulenburg, and Jonathan J. Ewbank. 2008. "Anti-Fungal Innate Immunity in C. Elegans Is Enhanced by Evolutionary Diversification of Antimicrobial Peptides." Edited by Frederick M. Ausubel. *PLoS Pathogens* 4 (7): e1000105. https://doi.org/10.1371/journal.ppat.1000105.

Qin, Li, Yanbo Nie, Hong Zhang, Long Chen, Donglei Zhang, Yani Lin, and Kun Ru. 2020. "Identification of New Mutations in Patients with Hereditary Spherocytosis by Next-Generation Sequencing." *Journal of Human Genetics* 65 (4): 427–34. https://doi.org/10.1038/s10038-020-0724-z.

Rajagopal, Abbhirami, Anita U. Rao, Julio Amigo, Meng Tian, Sanjeev K. Upadhyay, Caitlin Hall, Suji Uhm, et al. 2008. “Haem Homeostasis Is Regulated by the Conserved and Concerted Functions of HRG-1 Proteins.” *Nature* 453 (7198): 1127–31. https://doi.org/10.1038/nature06934.

Rajesh, Sundaresan, Ružica Bago, Elena Odintsova, Gayrat Muratov, Gouri Baldwin, Pooja Sridhar, Sandya Rajesh, Michael Overduin, and Fedor Berditchevski. 2011. “Binding to Syntenin-1 Protein Defines a New Mode of Ubiquitin-Based Interactions Regulated by Phosphorylation.” *The Journal of Biological Chemistry* 286 (45): 39606–14. https://doi.org/10.1074/jbc.M111.262402.

Ruiz, Lidia, Magali Traskine, Irene Ferrer, Estrella Castro, Juan F. M. Leal, Marcelline Kaufman, and Amancio Carnero. 2008. “Characterization of the P53 Response to Oncogene-Induced Senescence.” Edited by Mikhail V. Blagosklonny. *PLoS ONE* 3 (9): e3230. https://doi.org/10.1371/journal.pone.0003230.

Sánchez-Martín, Pablo, and Masaaki Komatsu. 2018. “P62/SQSTM1 – Steering the Cell through Health and Disease.” *Journal of Cell Science* 131 (21): jcs222836. https://doi.org/10.1242/jcs.222836.

Schmeisser, Sebastian, Steffen Priebe, Marco Groth, Shamci Monajembashi, Peter Hemmerich, Reinhard Guthke, Matthias Platzer, and Michael Ristow. 2013. “Neuronal ROS Signaling Rather than AMPK/Sirtuin-Mediated Energy Sensing Links Dietary Restriction to Lifespan Extension.” *Molecular Metabolism* 2 (2): 92–102. https://doi.org/10.1016/j.molmet.2013.02.002.

Schott, Geraldine, and Mariano A. Garcia-Blanco. 2020. “MHC Class III RNA Binding Proteins and Immunity.” *RNA Biology*, December, 1–7. https://doi.org/10.1080/15476286.2020.1860388.

Shuai, Ping, Zimeng Ye, Yuping Liu, Chao Qu, Xiaoqi Liu, Huaichao Luo, Xiaoyun Feng, Xiulan Li, Yi Shi, and Bo Gong. 2017. “Association between *SKIV2L* Polymorphism Rs429608 and Age-Related Macular Degeneration: A Meta-Analysis.” *Ophthalmic Genetics* 38 (3): 245–51. https://doi.org/10.1080/13816810.2016.1210650.

Silva, Joana V., Maria J. Freitas, and Margarida Fardilha. 2014. “Phosphoprotein Phosphatase 1 Complexes in Spermatogenesis.” *Current Molecular Pharmacology* 7 (2): 136–46. https://doi.org/10.2174/1874467208666150126154222.

Spracklen, Cassandra N., Momoko Horikoshi, Young Jin Kim, Kuang Lin, Fiona Bragg, Sanghoon Moon, Ken Suzuki, et al. 2020. “Identification of Type 2 Diabetes Loci in 433,540 East Asian Individuals.” *Nature* 582 (7811): 240–45. https://doi.org/10.1038/s41586-020-2263-3.

Staub, Eike, Joern Groene, Maya Heinze, Detlev Mennerich, Stefan Roepcke, Irina Klaman, Bernd Hinzmann, et al. 2009. “An Expression Module of WIPF1-Coexpressed Genes Identifies Patients with Favorable Prognosis in Three Tumor Types.” *Journal of Molecular Medicine* 87 (6): 633–44. https://doi.org/10.1007/s00109-009-0467-y.

Stranahan, Alexis M., Bronwen Martin, Wayne Chadwick, Sung-Soo Park, Liyun Wang, Kevin G. Becker, William H. Woodiii, Yongqing Zhang, and Stuart Maudsley. 2012. “Metabolic Context Regulates Distinct Hypothalamic Transcriptional Responses to Antiaging Interventions.” *International Journal of Endocrinology* 2012: 732975. https://doi.org/10.1155/2012/732975.

Struckmann, Stephan, Mathias Ernst, Sarah Fischer, Nancy Mah, Georg Fuellen, and Steffen Möller. 2020. “Scoring Functions for Drug-Effect Similarity.” *Briefings in Bioinformatics*, June, bbaa072. https://doi.org/10.1093/bib/bbaa072.

Stuart, Charles A., William L. Stone, Mary E. A. Howell, Marianne F. Brannon, H. Kenton Hall, Andrew L. Gibson, and Michael H. Stone. 2016. “Myosin Content of Individual Human Muscle Fibers Isolated by Laser Capture Microdissection.” *American Journal of Physiology-Cell Physiology* 310 (5): C381–89. https://doi.org/10.1152/ajpcell.00317.2015.

Sun, Hongze, Baochi Ou, Senlin Zhao, Xueni Liu, Liwei Song, Xisheng Liu, Rangrang Wang, and Zhihai Peng. 2019. “USP11 Promotes Growth and Metastasis of Colorectal Cancer via PPP1CA-Mediated Activation of ERK/MAPK Signaling Pathway.” *EBioMedicine* 48 (October): 236–47. https://doi.org/10.1016/j.ebiom.2019.08.061.

Szklarczyk, Damian, Annika L. Gable, Katerina C. Nastou, David Lyon, Rebecca Kirsch, Sampo Pyysalo, Nadezhda T. Doncheva, et al. 2021. “The STRING Database in 2021: Customizable

Protein-Protein Networks, and Functional Characterization of User-Uploaded Gene/Measurement Sets." *Nucleic Acids Research* 49 (D1): D605–12. https://doi.org/10.1093/nar/gkaa1074.

Tacutu, Robi, Thomas Craig, Arie Budovsky, Daniel Wuttke, Gilad Lehmann, Dmitri Taranukha, Joana Costa, Vadim E. Fraifeld, and João Pedro de Magalhães. 2012. "Human Ageing Genomic Resources: Integrated Databases and Tools for the Biology and Genetics of Ageing." *Nucleic Acids Research* 41 (D1): D1027–33. https://doi.org/10.1093/nar/gks1155.

Tacutu, Robi, Daniel Thornton, Emily Johnson, Arie Budovsky, Diogo Barardo, Thomas Craig, Eugene Diana, et al. 2018. "Human Ageing Genomic Resources: New and Updated Databases." *Nucleic Acids Research* 46 (D1): D1083–90. https://doi.org/10.1093/nar/gkx1042.

van Dam, Sipko, Thomas Craig, and João Pedro de Magalhães. 2015. "GeneFriends: A Human RNA-Seq-Based Gene and Transcript Co-Expression Database." *Nucleic Acids Research* 43 (D1): D1124–32. https://doi.org/10.1093/nar/gku1042.

Vardi, Iddo, Ortal Barel, Michal Sperber, Michael Schvimer, Moran Nunberg, Michael Field, Jodie Ouahed, et al. 2018. "Genetic and Structural Analysis of a SKIV2L Mutation Causing Tricho-Hepato-Enteric Syndrome." *Digestive Diseases and Sciences* 63 (5): 1192–99. https://doi.org/10.1007/s10620-018-4983-x.

Visvikis, Orane, Nnamdi Ihuegbu, Sid A. Labed, Lyly G. Luhachack, Anna-Maria F. Alves, Amanda C. Wollenberg, Lynda M. Stuart, Gary D. Stormo, and Javier E. Irazoqui. 2014. "Innate Host Defense Requires TFEB-Mediated Transcription of Cytoprotective and Antimicrobial Genes." *Immunity* 40 (6): 896–909. https://doi.org/10.1016/j.immuni.2014.05.002.

Wang, Lu, Zhen Li, David Sievert, Desirée E. C. Smith, Marisa I. Mendes, Dillon Y. Chen, Valentina Stanley, et al. 2020. "Loss of NARS1 Impairs Progenitor Proliferation in Cortical Brain Organoids and Leads to Microcephaly." *Nature Communications* 11 (1): 4038. https://doi.org/10.1038/s41467-020-17454-4.

Waters, Katherine, Alison Z. Yang, and Valerie Reinke. 2010. "Genome-Wide Analysis of Germ Cell Proliferation in C. Elegans Identifies VRK-1 as a Key Regulator of CEP-1/P53." *Developmental Biology* 344 (2): 1011–25. https://doi.org/10.1016/j.ydbio.2010.06.022.

Wu, Ping, Tingting Xiang, Jing Wang, Run Lv, and Guangzhen Wu. 2020. "*TYROBP* Is a Potential Prognostic Biomarker of Clear Cell Renal Cell Carcinoma." *FEBS Open Bio* 10 (12): 2588–2604. https://doi.org/10.1002/2211-5463.12993.

Yang, H., Y. Zhang, J. Vallandingham, H. Li, L. Florens, and H. Y. Mak. 2012. "The RDE-10/RDE-11 Complex Triggers RNAi-Induced MRNA Degradation by Association with Target MRNA in C. Elegans." *Genes & Development* 26 (8): 846–56. https://doi.org/10.1101/gad.180679.111.

Yates, Andrew D, Premanand Achuthan, Wasiu Akanni, James Allen, Jamie Allen, Jorge Alvarez-Jarreta, M Ridwan Amode, et al. 2019. "Ensembl 2020." *Nucleic Acids Research*, November, gkz966. https://doi.org/10.1093/nar/gkz966.

Zahn, Jacob M, Suresh Poosala, Art B Owen, Donald K Ingram, Ana Lustig, Arnell Carter, Ashani T Weeraratna, et al. 2007. "AGEMAP: A Gene Expression Database for Aging in Mice." Edited by Wayne N Frankel. *PLoS Genetics* 3 (11): e201. https://doi.org/10.1371/journal.pgen.0030201.

Zhang, Minhua, Michal Poplawski, Kelvin Yen, Hui Cheng, Erik Bloss, Xiao Zhu, Harshil Patel, and Charles V. Mobbs. 2009. "Role of CBP and SATB-1 in Aging, Dietary Restriction, and Insulin-Like Signaling." Edited by Andy Dillin. *PLoS Biology* 7 (11): e1000245. https://doi.org/10.1371/journal.pbio.1000245.

Zhang, Tao, Xiaopei Shen, Rengyun Liu, Guangwu Zhu, Justin Bishop, and Mingzhao Xing. 2017. "Epigenetically Upregulated WIPF1 Plays a Major Role in BRAF V600E-Promoted Papillary Thyroid Cancer Aggressiveness." *Oncotarget* 8 (1): 900–914. https://doi.org/10.18632/oncotarget.13400.

Zhang, Xingqian, Xiangwei Gao, Ryan Alex Coots, Crystal S Conn, Botao Liu, and Shu-Bing Qian. 2015. "Translational Control of the Cytosolic Stress Response by Mitochondrial Ribosomal Protein L18."

Nature Structural & Molecular Biology 22 (5): 404–10. https://doi.org/10.1038/nsmb.3010.

Zhao, Wei, Peter Langfelder, Tova Fuller, Jun Dong, Ai Li, and Steve Hovarth. 2010. “Weighted Gene Coexpression Network Analysis: State of the Art.” *Journal of Biopharmaceutical Statistics* 20 (2): 281–300. https://doi.org/10.1080/10543400903572753.

Supplement

Figures

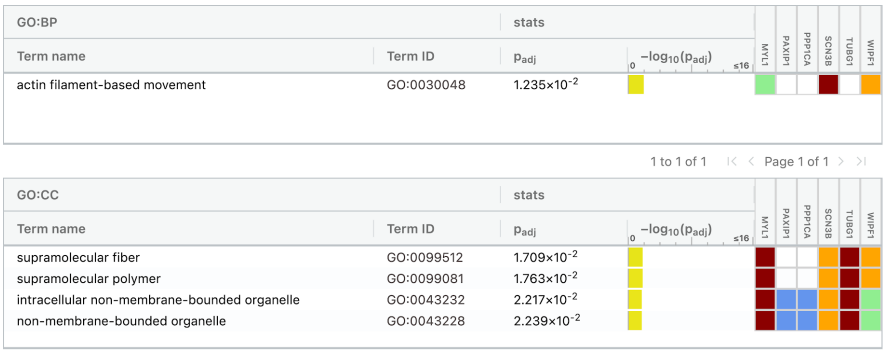

Supplement Figure 1a: g:profiler gene set enrichment analysis of genes listed jointly in Tables 2 and 3.

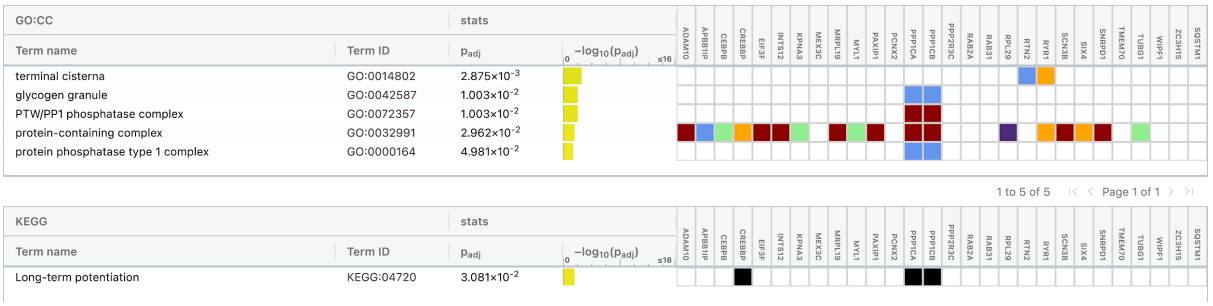

Supplement Figure 1b: g:profiler gene set enrichment analysis of genes listed in Table 3.

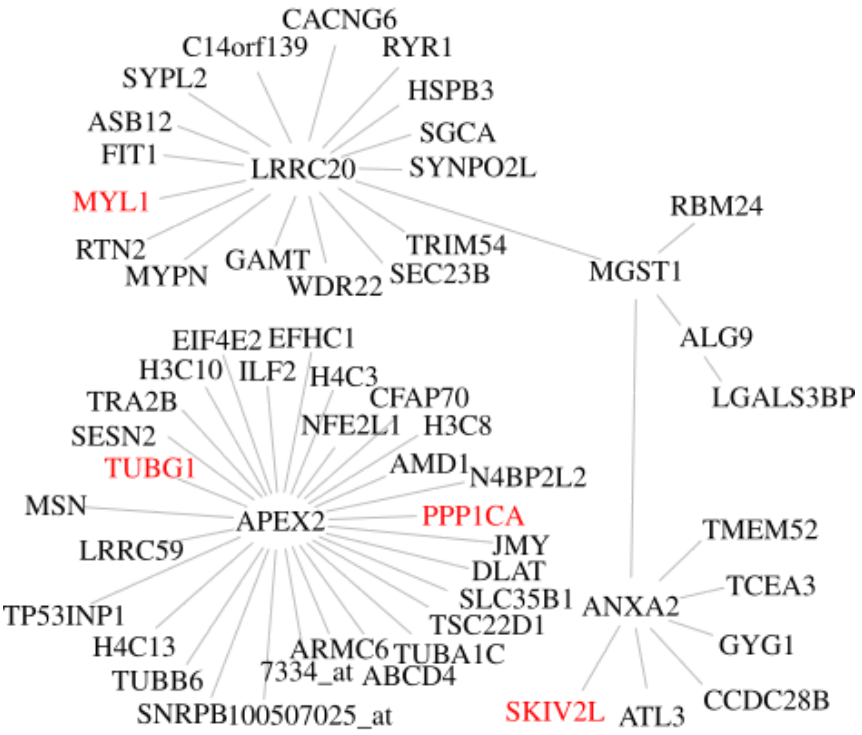

Supplement Figure 2a: Gene interactions observed in human. *The genes MYL1, PPP1CA, SKIV2L and TUBG1 are hub genes in WGCNA-defined modules from multiple species (cf. Figure 1, here shown in red). This graph was created iteratively with the red genes as a seed, then adding all the gene-gene interactions from WGCNA in human experiments originating from these red genes, and then transitively adding all the interacting genes of those. The resulting graph is highly interconnected before applying the minimum spanning tree algorithm. The genes interacting with hub genes across species (in red) then appear marginalized by the three human-only hub genes ANXA2, APEX2, LRRC20 and MGST1, given that the minimum spanning tree shows only the strongest correlations. ANXA2 is well described for a wide array of disease, i.e. cancer but also pulmonary fibrosis, and on a molecular level chimes in with vesicle fusion. APEX2 is a nuclease required for lymphocyte proliferation. LRRC20 is not yet described but known to interact with the also mostly undescribed TOM1 that once more is thought to be involved in intracellular trafficking and the E3 SUMO-protein ligase ZBED1. MGST1 is an enzyme located at the ER and mitochondria, a transferase of glutathione, an antioxidant.*

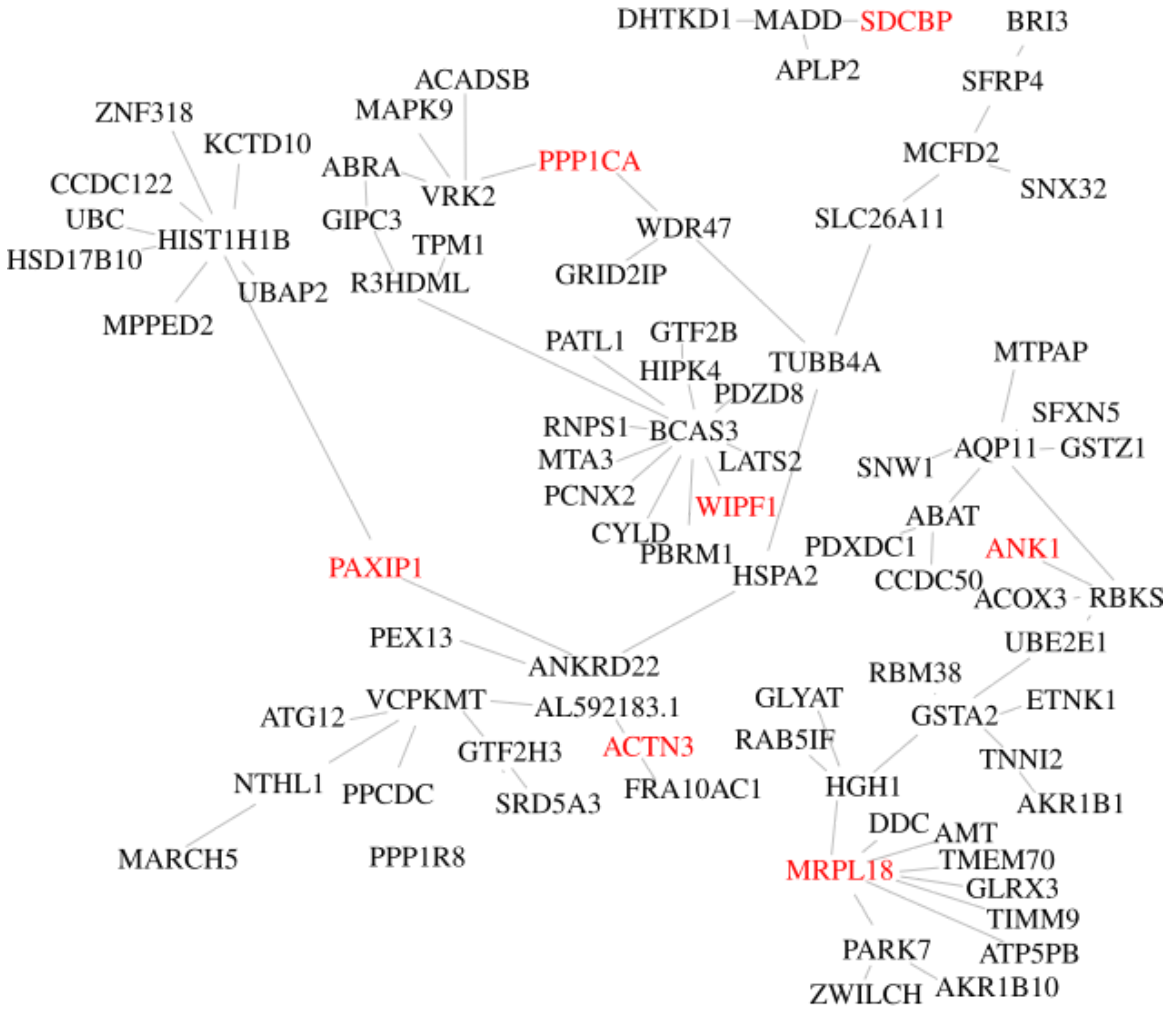

Supplement Figure 2b: *Gene interactions observed in worm. The figure was prepared analogously to Supplement Figure 2a from gene interactions observed in the worm. Gene names were mapped to human orthologs for an easier comparison between species.*

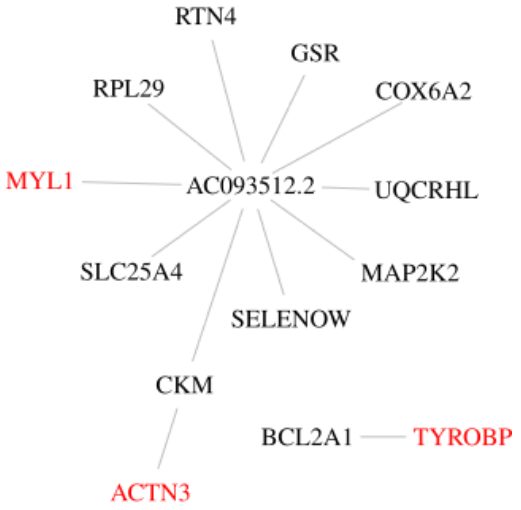

Supplement Figure 2c: Gene interactions observed in rat.

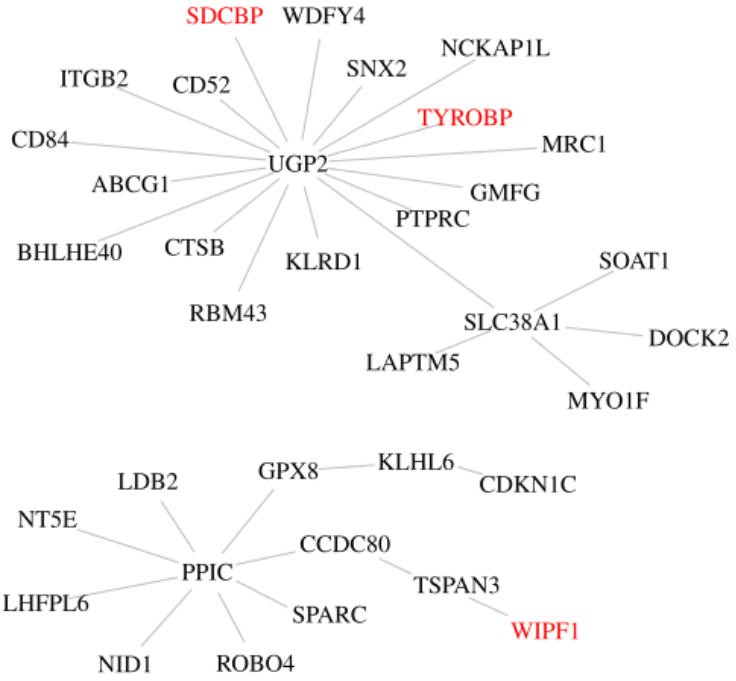

Supplement Figure 2d: Gene interactions observed in mouse.

Supplement Figure 3a: g:Profiler GSEA on genes connecting hub genes TYROBP and SDCBP.

Supplement Figure 3b: g:Profiler GSEA on genes connecting hub genes MYL1 and SKIV2L.

Supplement Figure 3c: g:Profiler GSEA on genes connecting hub genes TUBG1 and PPP1CA.

Tables

Supplement Table 1: Genes correlating with eigengene representation (module membership) *of those modules that are correlating with the health score. The table lists all genes that appear in at least two experiments among the top 30 and a P value below 0.05. If the expression of the gene correlates positively with the health score then the gene is tagged as positive. The columns "cor" and "P val" list the values as determined by WGCNA. A negative correlation with a positive tag indicates that eigengene of the module is negatively correlated with the health score.*

Gene	health	cor	P val	Experiment	module
0610006I08Rik	negative	0.907	4.64e-05	E-GEOD-19102	darkmagenta
0610006I08Rik	negative	0.942	4.57e-06	E-GEOD-19102	skyblue3
2010107E04Rik	positive	0.951	6.24e-19	E-GEOD-55272	black
2010107E04Rik	positive	-0.947	2.10e-18	E-GEOD-55272	magenta
ABAT	positive	0.988	2.21e-18	E-GEOD-30505	blue
ABAT	positive	-0.980	1.42e-12	E-GEOD-42192	turquoise
ABCG1	negative	-0.900	6.76e-05	E-GEOD-19102	sienna2
ABCG1	negative	0.974	1.68e-23	E-GEOD-55272	red
ABRA	negative	0.996	4.41e-12	E-GEOD-43864	brown
ABRA	negative	0.989	2.90e-06	E-GEOD-57739	turquoise
ABRA	positive	-0.968	1.12e-14	E-MTAB-1333	blue
abu-14	positive	0.993	5.68e-21	E-GEOD-30505	turquoise
abu-14	positive	0.999	7.55e-07	E-GEOD-9246	turquoise
AC068831.7	negative	-0.868	2.48e-04	E-GEOD-19102	yellow3
AC068831.7	negative	0.986	1.28e-18	E-MTAB-1333	turquoise
AC106774.4	negative	-0.873	2.13e-04	E-MEXP-1810	plum1
AC106774.4	negative	0.938	6.73e-06	E-MEXP-1810	royalblue
ADAM10	negative	-0.871	7.20e-09	E-GEOD-34773	greenyellow
ADAM10	positive	0.998	4.87e-13	E-GEOD-43864	turquoise
AGO1	negative	-0.995	2.14e-09	E-GEOD-32339	blue
AGO1	negative	-0.879	1.53e-08	E-MTAB-1333	black
ain-1	negative	0.921	4.24e-04	E-GEOD-8696	cyan
ain-1	negative	0.965	2.56e-05	E-GEOD-8696	royalblue
APBB1IP	positive	0.987	2.78e-09	E-GEOD-54853-CEL	yellow
APBB1IP	negative	0.970	1.68e-07	E-MTA-B6578	blue
AQP11	positive	0.997	2.57e-24	E-GEOD-30505	blue
AQP11	negative	0.951	1.98e-06	E-MEXP-1810	brown
ARMC1	positive	-0.850	3.97e-08	E-GEOD-34773	darkgrey
ARMC1	positive	0.874	5.48e-09	E-GEOD-34773	greenyellow
asns-2	negative	-0.993	7.01e-05	E-GEOD-51502	black
asns-2	positive	0.984	8.21e-09	EGEOD54853-CEL	brown
ATP6V1B2	negative	0.978	4.00e-08	E-GEOD-43864	paleturquoise
ATP6V1B2	negative	0.967	2.76e-07	E-GEOD-43864	paleturquoise
ATP6V1B2	positive	0.999	2.07e-06	E-GEOD-9246	turquoise
B2M	negative	0.927	1.03e-11	E-GEOD-34773	lightyellow
B2M	negative	0.922	2.13e-11	E-GEOD-34773	lightyellow
B2M	negative	0.975	6.82e-08	EMTAB6578	blue
C02E7.6	positive	0.993	4.20e-21	E-GEOD-30505	turquoise
C02E7.6	positive	0.990	9.63e-10	E-GEOD-43864	yellow
C09B9.2	negative	0.990	2.56e-06	E-GEOD-57739	turquoise
C09B9.2	positive	0.989	1.36e-19	E-MTAB-1333	yellow
C26F1.1	positive	0.989	1.13e-09	E-GEOD-43864	yellow
C26F1.1	negative	0.982	4.60e-04	E-GEOD-51502	turquoise

C46F2.1	negative	-0.869	2.45e-04	E-MEXP-1810	plum1
C46F2.1	negative	0.921	2.15e-05	E-MEXP-1810	royalblue
C46G7.1	positive	-0.979	1.62e-12	E-GEOD-42192	turquoise
C46G7.1	negative	0.928	8.98e-04	E-GEOD-57739	darkgreen
CAD	negative	-0.875	1.93e-04	E-MEXP-1810	plum1
CAD	negative	0.902	6.02e-05	E-MEXP-1810	royalblue
CD151	negative	0.934	8.51e-06	E-GEOD-19102	darkmagenta
CD151	negative	-0.905	2.28e-10	E-GEOD-34773	tan
CEBPB	positive	0.940	1.65e-04	E-GEOD-38062	salmon
CEBPB	negative	0.812	5.27e-08	E-GEOD-40936	grey
CLIC5	negative	0.842	6.00e-04	E-GEOD-19102	green3
CLIC5	negative	-0.883	2.42e-09	E-GEOD-34773	greenyellow
comp-1	negative	0.991	2.09e-06	E-GEOD-57739	turquoise
comp-1	positive	0.991	9.50e-21	E-MTAB-1333	yellow
COX15	positive	-0.890	1.19e-09	E-GEOD-34773	darkgrey
COX15	positive	-0.879	3.61e-09	E-GEOD-34773	darkgrey
COX15	positive	0.923	1.79e-11	E-GEOD-34773	greenyellow
cpg-2	negative	-0.994	5.19e-09	E-GEOD-32339	blue
cpg-2	positive	0.961	3.76e-05	E-GEOD-8696	red
CRB1	negative	-0.958	1.85e-04	E-GEOD-57739	darkorange
CRB1	positive	0.989	1.48e-09	EGEOD54853-CEL	yellow
CREBBP	negative	0.953	1.96e-05	E-GEOD-32339	pink
CREBBP	negative	0.937	1.75e-12	E-GEOD-34773	red
CREBBP	negative	0.958	4.89e-05	E-GEOD-8696	purple
D2062.7	positive	-0.969	4.07e-11	E-GEOD-42192	blue
D2062.7	positive	0.985	1.99e-18	E-MTAB-1333	yellow
DCP2	negative	0.928	1.74e-10	E-GEOD-30505	black
DCP2	negative	-0.997	2.13e-10	E-GEOD-32339	blue
DDX4	positive	-0.998	3.10e-13	E-GEOD-43864	blue
DDX4	negative	-0.877	1.77e-04	E-MEXP-1810	lightcyan
DEPDC1B	negative	0.915	9.48e-10	E-GEOD-30505	black
DEPDC1B	positive	-0.934	2.28e-04	E-GEOD-8696	cyan
dnj-3	positive	0.940	5.49e-06	E-GEOD-43864	royalblue
dnj-3	negative	0.924	1.05e-03	E-GEOD-57739	darkgreen
dnj-3	negative	0.974	9.23e-16	E-MTAB-1333	brown
DRG1	negative	0.993	6.92e-05	E-GEOD-51502	turquoise
DRG1	negative	0.925	1.64e-05	E-MEXP-1810	brown
EEF1B2	negative	-0.866	2.71e-04	E-GEOD-19102	deeppink
EEF1B2	positive	0.948	1.93e-13	E-GEOD-34773	green
egg-2	positive	-0.998	8.73e-14	E-GEOD-43864	blue
egg-2	positive	-0.998	2.95e-13	E-GEOD-43864	blue
egg-2	positive	0.964	2.85e-05	E-GEOD-8696	red
EIF3F	positive	-0.929	7.24e-12	E-GEOD-34773	purple
EIF3F	positive	0.999	9.64e-07	E-GEOD-9246	turquoise
EMC3	negative	-0.915	5.49e-04	E-GEOD-38062	darkgreen
EMC3	negative	0.954	6.54e-05	E-GEOD-38062	plum1
F45D3.4	positive	0.935	8.05e-06	E-MEXP-1810	darkmagenta
F45D3.4	positive	-0.917	2.69e-05	E-MEXP-1810	royalblue
F55A3.2	positive	0.867	2.62e-04	E-MEXP-1810	darkmagenta
F55A3.2	positive	0.876	1.89e-04	E-MEXP-1810	darkolivegreen
FBLN7	negative	0.877	1.83e-04	E-GEOD-19102	green3
FBLN7	negative	0.909	1.37e-10	E-GEOD-34773	magenta
fkb-7	positive	-0.995	4.39e-05	E-GEOD-51502	turquoise
fkb-7	positive	0.965	1.05e-04	E-GEOD-57739	sienna3

flp-15	positive	0.959	8.29e-07	E-MEXP-1810	plum1
flp-15	positive	0.914	3.14e-05	E-MEXP-1810	plum1
flp-15	positive	-0.898	7.43e-05	E-MEXP-1810	royalblue
GMFG	negative	0.892	9.67e-05	E-GEOD-19102	darkmagenta
GMFG	negative	0.984	6.89e-27	E-GEOD-55272	red
GNG10	negative	0.927	1.40e-05	E-GEOD-19102	darkmagenta
GNG10	positive	0.959	3.66e-20	E-GEOD-55272	yellow
GPR142	negative	0.990	7.71e-10	E-GEOD-43864	lightgreen
GPR142	negative	0.979	3.46e-08	E-GEOD-43864	lightgreen
GPR142	negative	0.925	3.56e-04	E-GEOD-8696	cyan
grl-7	positive	0.992	4.32e-20	E-GEOD-30505	turquoise
grl-7	positive	0.993	1.22e-10	E-GEOD-43864	yellow
grl-7	positive	0.991	3.61e-10	E-GEOD-43864	yellow
grl-7	positive	0.991	3.91e-10	E-GEOD-43864	yellow
GSTA2	positive	0.992	3.59e-20	E-GEOD-30505	blue
GSTA2	negative	0.976	6.93e-06	E-GEOD-8696	purple
GSTA2	negative	0.953	1.73e-06	E-MEXP-1810	brown
H2-D1	negative	0.951	9.09e-14	E-GEOD-34773	lightyellow
H2-D1	negative	0.948	1.95e-13	E-GEOD-34773	lightyellow
H2-D1	negative	0.941	9.01e-13	E-GEOD-34773	lightyellow
H2-D1	negative	0.894	7.30e-10	E-GEOD-34773	lightyellow
H2-D1	negative	0.974	9.03e-08	EMTAB6578	blue
H42K12.3	positive	0.992	2.23e-20	E-GEOD-30505	turquoise
H42K12.3	positive	0.988	2.15e-04	E-GEOD-51502	blue
HACL1	positive	0.881	1.55e-04	E-MEXP-1810	plum1
HACL1	positive	-0.963	5.25e-07	E-MEXP-1810	royalblue
HACL1	positive	-0.908	4.46e-05	E-MEXP-1810	royalblue
HSDL2	positive	0.940	5.23e-04	E-GEOD-57739	darkorange
HSDL2	positive	0.949	2.39e-06	E-MEXP-1810	lightcyan
IHH	negative	0.933	2.34e-04	E-GEOD-8696	cyan
IHH	positive	0.999	2.32e-06	E-GEOD-9246	turquoise
INTS12	negative	-0.845	5.42e-04	E-GEOD-19102	yellow3
INTS12	positive	-0.980	2.32e-08	E-GEOD-43864	paleturquoise
K08C9.2	negative	0.997	8.50e-13	E-GEOD-43864	brown
K08C9.2	positive	0.986	1.88e-18	E-MTAB-1333	yellow
KPNA3	negative	0.932	4.18e-12	E-GEOD-34773	red
KPNA3	positive	0.999	2.92e-06	E-GEOD-9246	turquoise
let-2	positive	0.992	1.36e-20	E-GEOD-30505	blue
let-2	positive	-0.979	1.83e-12	E-GEOD-42192	turquoise
LIAS	positive	-0.921	2.67e-11	E-GEOD-34773	black
LIAS	positive	0.880	3.27e-09	E-GEOD-34773	tan
LIN28A	positive	-0.998	1.06e-13	E-GEOD-43864	blue
LIN28A	positive	-0.998	2.15e-13	E-GEOD-43864	blue
LIN28A	negative	-0.877	1.78e-04	E-MEXP-1810	darkolivegreen
MARCKS	negative	0.967	3.10e-07	E-GEOD-19102	blue
MARCKS	negative	0.918	4.08e-11	E-GEOD-34773	magenta
MEX3C	negative	-0.994	7.28e-09	E-GEOD-32339	blue
MEX3C	negative	0.948	6.71e-13	E-GEOD-38012	yellow
mig-6	positive	-0.978	2.21e-12	E-GEOD-42192	turquoise
mig-6	positive	0.984	8.04e-09	EGEOD54853-CEL	yellow
MRAS	positive	0.989	5.85e-19	E-GEOD-30505	blue
MRAS	positive	-0.965	3.01e-14	E-MTAB-1333	blue
MRPL13	positive	-0.886	1.74e-09	E-GEOD-34773	darkgrey
MRPL13	positive	-0.878	3.75e-09	E-GEOD-34773	darkgrey

MRPL13	positive	0.867	9.86e-09	E-GEOD-34773	greenyellow
MRPL19	positive	-0.869	8.64e-09	E-GEOD-34773	darkgrey
MRPL19	negative	0.951	1.96e-06	E-MEXP-1810	brown
MRPL30	negative	0.888	1.13e-04	E-GEOD-19102	skyblue3
MRPL30	positive	0.939	2.45e-17	E-GEOD-55272	black
MTPAP	negative	-0.992	3.65e-20	E-GEOD-30505	blue
MTPAP	negative	-0.995	2.69e-09	E-GEOD-32339	blue
Myeov2	positive	0.931	1.71e-16	E-GEOD-55272	black
Myeov2	positive	-0.976	5.77e-24	E-GEOD-55272	magenta
MYL1	positive	-0.996	3.24e-25	E-GEOD-38012	turquoise
MYL1	positive	0.985	1.49e-06	E-GEOD-38062	tan
MYL7	negative	0.895	8.28e-05	E-GEOD-19102	skyblue3
MYL7	negative	0.901	6.40e-05	EGEOD54853-MMU	darkturquoise
NDUFS1	positive	0.862	3.07e-04	E-GEOD-19102	coral1
NDUFS1	positive	0.877	1.77e-04	E-GEOD-19102	lightsteelblue1
NR1H2	positive	0.983	1.22e-08	E-GEOD-43864	darkorange
NR1H2	negative	-0.909	1.75e-03	E-GEOD-57739	sienna3
NR1H2	positive	0.883	1.42e-04	E-MEXP-1810	darkolivegreen
NR1H2	positive	0.851	4.51e-04	E-MEXP-1810	darkolivegreen
NR1H2	positive	0.894	3.95e-09	E-MTAB-1333	black
NRBP1	negative	0.855	2.64e-08	E-GEOD-34773	darkgrey
NRBP1	negative	0.969	4.13e-22	E-GEOD-55272	pink
Pabpc1	positive	-0.887	1.21e-04	E-GEOD-19102	darkmagenta
Pabpc1	negative	0.969	2.22e-07	EMTAB6578	blue
PAXIP1	positive	0.890	1.03e-04	E-GEOD-19102	deeppink
PAXIP1	positive	0.998	2.67e-13	E-GEOD-43864	turquoise
PCNX2	negative	0.962	7.78e-14	E-MTAB-1333	blue
PCNX2	negative	0.907	4.66e-05	EGEOD54853-MMU	darkturquoise
PDCD6	negative	-0.959	8.71e-07	E-GEOD-43864	royalblue
PDCD6	negative	0.928	6.50e-11	E-MTAB-1333	green
PFAS	positive	-0.858	2.13e-08	E-GEOD-34773	darkgrey
PFAS	positive	0.941	8.58e-13	E-GEOD-34773	greenyellow
PPIA	positive	-0.975	6.83e-12	E-GEOD-42192	blue
PPIA	negative	0.918	2.52e-05	E-MEXP-1810	royalblue
PPIC	negative	0.981	1.67e-08	E-GEOD-19102	blue
PPIC	negative	0.981	1.97e-08	E-GEOD-19102	blue
PPIC	negative	0.917	4.55e-11	E-GEOD-34773	magenta
PPP1CA	positive	0.987	2.48e-04	E-GEOD-51502	black
PPP1CA	negative	0.991	1.68e-06	E-GEOD-57739	turquoise
PPP1CA	positive	0.993	2.02e-14	E-GEOD-66236	turquoise
PPP1CA	positive	0.989	9.26e-20	E-MTAB-1333	yellow
PPP1CB	positive	-0.979	4.67e-06	E-GEOD-38062	turquoise
PPP1CB	positive	0.999	1.18e-06	E-GEOD-9246	turquoise
PPP2R3C	negative	0.944	1.38e-12	E-GEOD-38012	yellow
PPP2R3C	negative	0.966	1.31e-21	E-GEOD-55272	pink
pqn-32	positive	0.993	3.79e-21	E-GEOD-30505	turquoise
pqn-32	positive	0.993	1.60e-10	E-GEOD-43864	yellow
pqn-32	positive	0.989	1.27e-09	E-GEOD-43864	yellow
PSMD4	positive	0.932	9.87e-06	E-GEOD-19102	lightpink2
PSMD4	negative	0.848	4.59e-08	E-GEOD-34773	darkgrey
ptp-2	negative	-0.937	7.07e-06	E-MEXP-1810	plum1
ptp-2	negative	0.932	1.03e-05	E-MEXP-1810	royalblue
PUM1	negative	-0.995	3.07e-09	E-GEOD-32339	blue
PUM1	negative	-0.995	3.51e-09	E-GEOD-32339	blue

PUM1	positive	0.986	9.40e-07	E-GEOD-8696	red
R3HDML	negative	-0.898	7.34e-05	E-MEXP-1810	plum1
R3HDML	negative	0.928	1.33e-05	E-MEXP-1810	royalblue
R3HDML	negative	0.916	2.80e-05	E-MEXP-1810	royalblue
RAB2A	negative	0.965	6.41e-06	E-GEOD-32339	pink
RAB2A	negative	0.960	2.47e-20	E-GEOD-55272	pink
RAB31	negative	0.952	1.77e-06	E-GEOD-19102	blue
RAB31	negative	0.971	1.37e-05	E-GEOD-38062	turquoise
RAD17	negative	0.994	5.90e-09	E-GEOD-32339	turquoise
RAD17	negative	0.982	1.90e-17	E-MTAB-1333	turquoise
RGL1	negative	0.956	1.25e-06	E-GEOD-19102	blue
RGL1	positive	-0.687	2.76e-05	E-GEOD-40936	grey
RMDN3	positive	-0.971	2.12e-11	E-GEOD-42192	blue
RMDN3	negative	0.999	3.97e-14	E-GEOD-43864	brown
RMDN3	negative	0.996	4.43e-12	E-GEOD-43864	brown
RMDN3	positive	0.967	2.03e-05	E-GEOD-8696	red
RPL11	positive	0.929	7.00e-12	E-GEOD-34773	green
RPL11	positive	0.963	7.42e-21	E-GEOD-55272	yellow
RPL13A	positive	0.936	2.43e-12	E-GEOD-34773	green
RPL13A	positive	-0.959	1.11e-14	E-GEOD-34773	purple
RPL23A	positive	0.934	3.34e-12	E-GEOD-34773	green
RPL23A	positive	0.929	7.50e-12	E-GEOD-34773	green
RPL23A	positive	-0.966	1.56e-15	E-GEOD-34773	purple
RPL23A	positive	-0.939	1.26e-12	E-GEOD-34773	purple
RPL23A	positive	-0.934	3.44e-12	E-GEOD-34773	purple
RPL27	positive	0.930	6.54e-12	E-GEOD-34773	green
RPL27	positive	-0.963	4.04e-15	E-GEOD-34773	purple
Rpl27a	positive	0.935	2.52e-12	E-GEOD-34773	green
Rpl27a	positive	0.965	2.64e-21	E-GEOD-55272	yellow
RPL29	positive	0.940	1.09e-12	E-GEOD-34773	green
RPL29	positive	0.976	7.35e-06	E-GEOD-38062	tan
RPS12	positive	0.942	7.63e-13	E-GEOD-34773	green
RPS12	positive	-0.926	1.28e-11	E-GEOD-34773	purple
RPS21	positive	0.954	4.18e-14	E-GEOD-34773	green
RPS21	positive	0.937	1.87e-12	E-GEOD-34773	green
RPS21	positive	-0.923	1.82e-11	E-GEOD-34773	purple
Rps25	positive	0.960	1.00e-14	E-GEOD-34773	green
Rps25	positive	-0.927	1.02e-11	E-GEOD-34773	purple
Rps29	positive	0.935	2.90e-12	E-GEOD-34773	green
Rps29	positive	-0.954	4.47e-14	E-GEOD-34773	purple
RPS7	negative	-0.905	5.22e-05	E-GEOD-19102	deeppink
RPS7	positive	-0.923	1.92e-11	E-GEOD-34773	purple
RTN2	negative	0.861	1.66e-08	E-GEOD-34773	darkgrey
RTN2	positive	-0.995	2.44e-24	E-GEOD-38012	turquoise
RYR1	positive	0.883	1.43e-04	E-GEOD-19102	sienna2
RYR1	positive	-0.994	2.21e-23	E-GEOD-38012	turquoise
SCN3B	positive	-0.879	1.67e-04	E-GEOD-19102	green3
SCN3B	positive	-0.956	5.85e-05	E-GEOD-38062	yellowgreen
SFT2D2	negative	-0.929	2.73e-16	E-GEOD-55272	black
SFT2D2	negative	0.975	8.14e-24	E-GEOD-55272	magenta
sgo-1	positive	-0.998	1.68e-13	E-GEOD-43864	blue
sgo-1	negative	0.985	3.18e-18	E-MTAB-1333	turquoise
SIK1B	negative	0.992	1.18e-06	E-GEOD-57739	turquoise
SIK1B	positive	0.989	1.13e-19	E-MTAB-1333	yellow

SIX4	negative	0.954	1.74e-12	E-GEOD-30505	red
SIX4	negative	-0.871	7.31e-09	E-GEOD-34773	greenyellow
SKP1	negative	0.995	2.19e-09	E-GEOD-32339	turquoise
SKP1	negative	0.940	9.01e-12	E-MTAB-1333	green
SKP1	negative	0.924	1.21e-10	E-MTAB-1333	green
SLC16A9	positive	0.989	1.02e-18	E-GEOD-30505	blue
SLC16A9	negative	-0.911	3.81e-05	E-MEXP-1810	darkmagenta
SLC7A11	negative	0.960	1.19e-13	E-MTAB-1333	blue
SLC7A11	positive	0.987	2.50e-09	EGEOD54853-CEL	brown
smz-2	positive	-0.970	3.19e-11	E-GEOD-42192	blue
smz-2	positive	0.988	2.18e-19	E-MTAB-1333	yellow
SNRPD1	negative	-0.875	1.91e-04	E-GEOD-19102	lightsteelblue1
SNRPD1	negative	0.954	6.08e-13	E-MTAB-1333	brown
somi-1	positive	0.917	2.74e-05	E-MEXP-1810	plum1
somi-1	positive	0.993	1.50e-10	EGEOD54853-CEL	yellow
spe-38	negative	-0.976	6.37e-08	E-GEOD-43864	darkorange
spe-38	negative	0.992	2.98e-10	E-GEOD-43864	lightgreen
SQSTM1	negative	0.959	1.07e-14	E-GEOD-34773	black
SQSTM1	negative	0.924	3.74e-04	E-GEOD-38062	yellowgreen
SQSTM1	positive	0.885	1.29e-04	E-MEXP-1810	lightcyan
sss-2	positive	-0.970	3.11e-11	E-GEOD-42192	blue
sss-2	positive	0.990	5.42e-20	E-MTAB-1333	yellow
T14G11.1	negative	-0.955	2.26e-04	E-GEOD-57739	darkorange
T14G11.1	negative	-0.909	7.81e-10	E-MTAB-1333	black
T19D12.2	negative	0.979	6.61e-04	E-GEOD-51502	turquoise
T19D12.2	positive	-0.892	9.42e-05	E-MEXP-1810	royalblue
T22B3.3	negative	0.998	3.30e-08	E-GEOD-57739	turquoise
T22B3.3	positive	0.989	1.42e-19	E-MTAB-1333	yellow
T28B11.1	positive	-0.928	1.39e-05	E-MEXP-1810	brown
T28B11.1	negative	0.964	3.65e-14	E-MTAB-1333	blue
T28H11.7	positive	-0.981	8.69e-13	E-GEOD-42192	blue
T28H11.7	positive	0.987	4.02e-19	E-MTAB-1333	yellow
TGIF2	negative	0.964	7.01e-06	E-GEOD-32339	pink
TGIF2	positive	0.883	1.08e-08	E-MTAB-1333	black
TMEM70	positive	-0.913	8.24e-11	E-GEOD-34773	darkgrey
TMEM70	negative	0.952	1.87e-06	E-MEXP-1810	brown
TNNI2	positive	0.905	5.22e-05	E-MEXP-1810	plum1
TNNI2	positive	0.870	2.34e-04	E-MEXP-1810	plum1
TNNI2	positive	0.992	3.43e-10	EGEOD54853-CEL	brown
TOMM70	positive	-0.917	2.70e-05	E-GEOD-19102	darkmagenta
TOMM70	positive	0.879	1.65e-04	E-GEOD-19102	deeppink
TUBG1	negative	0.948	1.03e-04	E-GEOD-38062	plum1
TUBG1	positive	0.987	1.43e-12	E-GEOD-66236	turquoise
UBE2E1	negative	-0.989	7.37e-19	E-GEOD-30505	blue
UBE2E1	negative	-0.993	8.90e-09	E-GEOD-32339	blue
UGT3A1	positive	-0.979	1.55e-12	E-GEOD-42192	turquoise
UGT3A1	positive	0.935	6.68e-04	E-GEOD-57739	sienna3
UTY	negative	0.986	2.97e-04	E-GEOD-51502	turquoise
UTY	positive	0.985	6.35e-09	EGEOD54853-CEL	yellow
VAMP3	negative	-0.912	9.32e-11	E-GEOD-34773	greenyellow
VAMP3	negative	-0.885	1.96e-09	E-GEOD-34773	tan
VRK2	positive	-0.972	1.70e-11	E-GEOD-42192	blue
VRK2	negative	-0.935	8.29e-06	E-GEOD-43864	darkorange
VRK2	negative	0.996	1.77e-07	E-GEOD-57739	turquoise

VRK2	negative	0.993	9.81e-07	E-GEOD-57739	turquoise
VRK2	negative	0.982	2.26e-17	E-MTAB-1333	turquoise
VRK2	positive	0.990	3.87e-20	E-MTAB-1333	yellow
VRK2	positive	0.989	1.44e-19	E-MTAB-1333	yellow
VRK2	positive	0.986	1.55e-18	E-MTAB-1333	yellow
W03G11.4	positive	0.993	1.43e-10	E-GEOD-43864	yellow
W03G11.4	positive	0.990	8.23e-10	E-GEOD-43864	yellow
W03G11.4	positive	0.998	3.84e-06	E-GEOD-9246	turquoise
W03G11.4	positive	0.990	6.47e-10	EGEOD54853-CEL	yellow
WDR47	negative	-0.993	6.36e-05	E-GEOD-51502	black
WDR47	positive	0.947	2.94e-06	E-MEXP-1810	darkmagenta
WIPF1	negative	0.954	1.55e-06	E-GEOD-19102	blue
WIPF1	negative	0.919	3.60e-11	E-GEOD-34773	magenta
WIPF1	negative	0.962	6.73e-14	E-MTAB-1333	blue
Y42H9AR.4	negative	0.942	2.15e-11	E-GEOD-30505	black
Y42H9AR.4	negative	-0.996	1.78e-09	E-GEOD-32339	blue
ZC3H15	negative	0.982	1.56e-08	E-GEOD-43864	midnightblue
ZC3H15	negative	-0.978	7.07e-25	E-GEOD-55272	yellow
ZFP36	negative	-0.994	4.29e-09	E-GEOD-32339	blue
ZFP36	negative	-0.994	4.60e-09	E-GEOD-32339	blue
ZFP36	positive	0.971	1.33e-05	E-GEOD-8696	red